Accepted Manuscript

Generation and assessment of local climatic data from numerical meteorological codes for calibration of building energy models

Fabiana Silvero

Please cite this article as: Fabiana Silvero , Generation and assessment of local climatic data from numerical meteorological codes for calibration of building energy models , *Energy & Buildings* (2019), doi: https://doi.org/10.1016/j.enbuild.2019.02.001

Generation and assessment of local climatic data from numerical meteorological codes for calibration of building energy models

ABSTRACT

The assessment of building energy performance through dynamic simulations has been increasing significantly in recent years since it represents a key strategy for the correct design of highly efficient buildings. Results of dynamic energy simulations are affected by many uncertainties, and its reliability depends on the accuracy of the input variables. One of the most influential variables is the climate surrounding the building, a reason why the use of accurate weather data files is essential, but experimental datasets are not always available. In this context, this paper analyses numerical weather datasets obtained from different regional climate models by comparing them with real data; in addition, it evaluates their impact on the energy performance of a historical building in Asunción through dynamic simulations. The database of five different weather data sources is compared with observed meteorological data in order to assess their accuracy through statistical analyses. Moreover, some methodologies to estimate diffused and direct components of the global solar radiation are evaluated, with the objective of solving the problem of missing direct and diffused solar data components from the meteorological codes. Subsequently, weather data files are generated to quantify the influence of measured/simulated meteorological data on the evaluation of building energy performance. The results obtained in this paper show that the simulated meteorological data agree very well with real observations for the year under study. Also, the simulations of the building energy performance delivered similar values to those obtained using the real weather dataset. Therefore, the regional climate models can represent a reliable tool for building energy performance assessment, and mainly for the calibration of building energy models when measured weather data is not available.

Keywords: Weather files; regional climate models; buildings energy simulation; thermal comfort; building energy demand.

Organisation

1. Introduction

According to the Fifth Assessment Report of the Intergovernmental Panel on Climate Change (IPCC), the building sector absorbed about 32% of total global final energy consumption in 2010, being one of the largest end-use sectors worldwide [1]. Generally, building energy use in developed countries is very wasteful and inefficient, and the risk that this tendency could be

diffused among developing countries is high. Thus, considering business-as-usual projections on a global level, energy use in the building sector can double or even triple by 2050 [2]. Considering this, Levine et al., [3] analysed the potential global reduction of greenhouse gas (GHG) emissions around the world for the building sector, through a review of several recent studies from different countries. By using the estimated CO_2 emission projections for the year 2020 as baseline, the authors found that there is a cost-effective global potential to reduce approximately 29% of these emissions in this sector, through the implementation of energy efficiency (EE) measures.

In recent years, the use of computational tools for the assessment of building energy performance has increased significantly since it represents a key strategy for the correct design of highly efficient buildings, as well as to quantify the potential energy savings in retrofit projects [4]. The general objective is to achieve the best indoor thermal comfort with minimum energy consumption, maintaining the quality of life with lower energy needs. Nonetheless, results of dynamic energy simulations are affected by many uncertainties (i.e. uncertainty of energy consumption calculation model) and its reliability depends on the accuracy of the input variables [5,6]. In this sense, ASHRAE Guideline 14-2002 "Measurement of Energy Demand Saving" suggests a calibration of the building simulation in order to reduce the overall error.

According to Radhi [7], three main factors impact a building energy use: climate, design and people; where the most influential factor seems to be the climate surrounding the building [8]. Weather data can normally be obtained using computational tools or from observed meteorological data of a weather station [9]. Unfortunately, the latter is not always available for every location of interest. For example, Paraguay has 23 meteorological stations in operation covering a total area of 406752 km^2, distributed in the main cities of the country. In fact, if evenly distributed, this would imply a meteorological station for every 17684 km^2, but this is not the case since three stations are located only in the capital, for example. This involves an important area in the country for which there are no measured meteorological data.

The computational tools are instead represented by software to generate weather data, which use statistical methods to generate detailed weather files on actual or past measured databases derived from a long period of recordings (usually 20-30 years), and which create a "typical meteorological year" (TMY) suitable to be used in building energy assessment. The databases are a comprehensive source of weather data covering several meteorological stations worldwide [10]. Some of these weather data generators are Meteonorm Software [11], TRNSYS [12], TRY Software [13], RUNEOLE [14] and so on. Two problems may arise regarding calibration of building energy models with these kinds of datasets: the unavailability of a reference weather file for the building location analysed or the availability of energy consumption data for a specific year that is far from the TMY average behaviour [5,7,15].

In this way, this paper aims to demonstrate that annual meteorological datasets obtained from regional climate models could represent a reliable option for the creation of weather data files to be used in the calibration of building energy models. Thus, a comparative analysis of weather datasets obtained from various climate models is adressed in this research, in order to evaluate

their accuracy in simulating the climate parameters under study. Subsequently, it evaluates their impact on building energy requirement and comfort conditions through dynamic simulations resourcing Energy Plus software and DesignBuilder interface. Therefore this research has three main stages briefly described below.

The first stage involves the intercomparison between weather datasets obtained from different sources. The climate parameters to compare are temperature, atmospheric pressure, relative humidity, wind speed, wind direction and cloud cover. The weather data sources used correspond to the Fifth Mesoscale Model (MM5), the HadRM3P and RCA4 regional models through the Coordinated Regional Climate Downscaling Experiment (CORDEX) and the International Weather for Energy Calculations (IWEC). The evaluation is made considering the correlation coefficient (R), the centered root-mean-square difference (RMSD) and the standard deviation (σ). This stage aims to figure out the accuracy of these climate models to describe the pattern of the analysed climate parameters and the climatology of the cities under study. To this purpose, the datasets are compared with observed meteorological data collected from a weather station.

In the second stage, some common methodologies to estimate the diffused and direct component of the global solar radiation are analysed, aiming to solve the problem of missing separated components and to evaluate the accuracy of the selected correlation models. The third stage consists in creating weather data files to be used in the building simulation software, with the objective of quantifying the influence of measured/simulated meteorological data on the evaluation of building energy performance.

This paper is structured as follows: after this introduction, a state of the art and background is briefly described in Section 2. The methodology employed is described in Section 3. Section 4 describes the weather data sources used for the present analysis and the methodology for the estimation of solar radiation data. Subsequently, Section 5 presents the intercomparison between the weather datasets. Section 6 describes the case study, defines the input parameters for the building dynamic energy simulations and presents the analysis of the results and discussions. Finally, Section 7 draws the main conclusions.

2. Background

Nowadays, within the framework of climate change issues, several climate models have been developed to simulate not only the future but also past climate conditions aiming to verify the accuracy of the model results. By addressing a hindcasting procedure, the weather data obtained through climate models can be used to create weather data files to simulate and evaluate the energy performance of buildings, in the absence of observed meteorological data.

Several scientific investigations have been developed to analyse the impact of weather data files in building energy simulations, as well as to calibrate and assess the accuracy of different weather data sources. Bhandari et al. [16] analysed the impact of climate parameters on building energy loads; it was found that monthly building loads can range by ±40% and annual energy consumption can vary by ±7% as a function of the weather data employed. Mahdavi et al. [5] demonstrated the

significant range of fluctuations in the simulated values of buildings' heating and cooling energy demands due to the

Nomenclature			
R	correlation coefficient	θ_Z	zenith angle of the sun [°]
RMSD	root-mean-square difference	s	thickness [m]
σ	standard deviation	λ	thermal conductivity [W/m K]
T	temperature [°C]	c	specific heat [J/Kg K]
P	atmospheric pressure [kPa]	ρ	density [Kg/ m^3]
RH	relative humidity [%]	U	thermal transmittance [W/m^2 K]
m	optical air mass number [-]	M_s	thermal mass [Kg/m^2]
P_o	atmospheric pressure at sea level [kPa]	R_t	thermal resistance [m^2 K/W]
α_s	solar altitude angle of the sun [°]	G_{sc}	global solar constant [W/m^2]
τ	atmospheric transmittance coefficient [-]	I_{gl}	global solar radiation [W/m^2]
ΔT	thermal amplitude [°C]	I_{dir}	direct solar radiation [W/m^2]
k_t	hourly clearness index [-]	I_{diff}	diffused solar radiation [W/m^2]
K_T	daily clearness index [-]	I_{ext}	extra-terrestrial solar radiation [W/m^2]
ψ	persistence factor [-]	I_p	direct radiation on a surface perpendicular to the beam [W/m^2]
d	diffused fraction [-]		

application of weather data from different locations for the city of Vienna, Austria.

Radhi [7] concluded that the weather files based on past data tend to underestimate electricity consumption by 14.5% and misrepresents the cooling load by 5.9–8.9%. Erba, et al. [17] evaluated 32 different combinations to identify the best energy retrofit solution for a building envelope, considering two different weather datasets, and obtained substantially different energy and comfort performance results. Ciobanu et al. [9] investigated the accuracy of weather datasets obtained from Meteonorm Software for the city of Brașov in Romania, concluding that the difference between the yearly heating need, calculated using the software database, and the value obtained based on the recorded weather data is approximately 20%.

Chiesa and Grosso [18] analysed a residential building located in three Italian cities using two different weather datasets. The results showed that the weather file influences the accuracy of predicted energy need especially in summer season. In addition, the result differences between the two different weather files reach nearly 17% for cooling and 39% for heating. Murphy et al. [19] investigated the effect on energy consumption estimation of a dwelling by varying climatic data using weather data for 14 locations across the United Kingdom. As a result, they showed that weather data could have a significant bearing on simulated kWh/year output, varying the calculated energy consumption by ±15%.

Thus, the creation of a reliable building model for dynamic simulations requires the specification of several parameters, such as envelope details, thermal properties of materials, operation schedules, etc., coupled with the choice of suitable weather

datasets, which better represents the climate surrounding the building [20]. Also, the calibration of building energy simulations must be an integral part of the modelling process [21] and several works also have analysed the uncertainties involved in calibration processes [22–24]. In general, real energy consumption data is the most used parameter to evaluate the accuracy of the outcomes, but inaccurate weather datasets can make the calibration process difficult [25]. In addition, real in situ measurements of temperature, relative humidity and other climate parameters inside the building can be recorded to perform the model calibration process. However, monitoring the outdoor conditions could be considered a more difficult task, and the availability of weather data from weather stations could be limited, as previously referred. Nonetheless, in order to fill this gap and allow the calibration of building energy models using weather data of the real site location, regional climate models can be resourced to simulate the outdoor weather conditions of the building. Therefore, the novelty of this research is based on the use of a hindcasting procedure using climate models in order to create a virtual weather station in every point of the globe for the calibration of building energy models. Thus, the present paper evaluates this procedure for a city located in the southern hemisphere.

3. Methodology

The work developed in the present investigation is summarised in Figure 1 and the methodology employed is described in the following subsections.
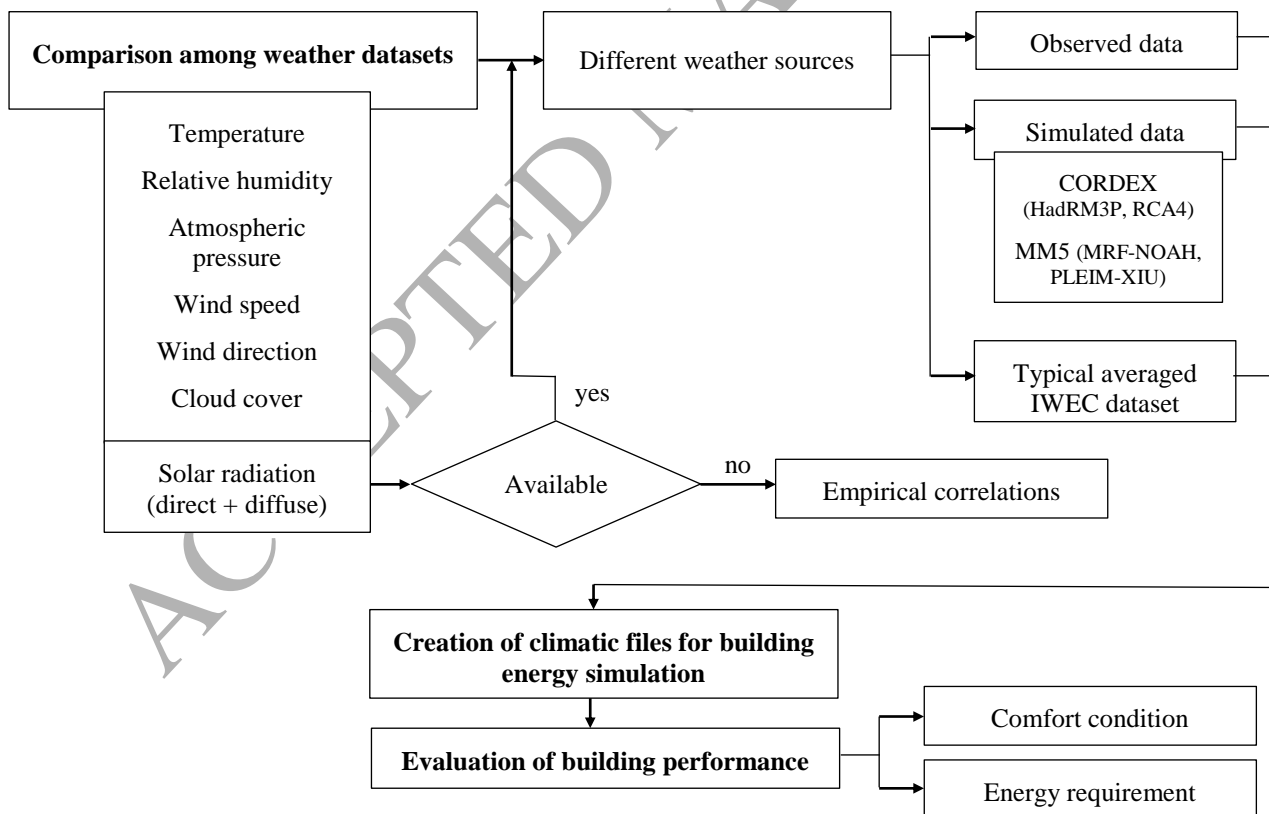

Figure 1 - Flowchart of the work developed in this paper.

3.1 Comparison of climate files

The first task of this paper is the comparison between observed and simulated climatic parameters. As was previously referred, one of the most difficult tasks for this type of work is the collection of observed meteorological data. The studied site location is the city of Asunción, Paraguay, for which it was possible to obtain observed data regarding six climate parameters (temperature, atmospheric pressure, relative humidity, wind speed, wind direction and cloud cover) from the mast in the Silvio Pettirossi Airport. As solar radiation data is not recorded in the mast but has a significant impact on the energy simulations of buildings, and it is an essential climatic parameter for the creation of weather data files, a derived estimation of this parameter and its components for Asunción was described and adopted. This estimation was made considering the sun angles and position, the latitude and longitude of the site location, and the extra-terrestrial radiation on a horizontal surface. The datasets for the solar radiation obtained from this methodology were used to create the reference experimental weather file of Asunción for the subsequent energy simulations. The methodology for the estimation is fully described in subsection 2.1.5.

3.2 Application of correlation models to estimate solar radiation components

The lack of solar information in the Asunción meteorological mast and the need to analyse the accuracy of the solar radiation outputs obtained from the climate models (CORDEX and MM5) led to the selection of observed real data regarding solar radiation from another meteorological mast; in particular from the city of São Martinho da Serra (Brazil). It is important to highlight that meteorological masts recording solar information data in Paraguay are scarce, while solar information data for this Brazilian city was chosen considering the amount and the quality of the available data validated through a quality control process. Indeed, this source [26] has also been used to create and validate several correlation models for the estimation of solar radiation data (models reviewed in section 2.1.5). Even though these correlation models can be applied to any location in the world, according to the authors, it is important to note that Asunción and São Martinho da Serra are in the same climatic area, in the same hemisphere and 750 km far from each other. In this way, it was possible to compare all the datasets obtained from the estimation model and the climate models using observed data for solar radiation components. The correlation model which better agreed with São Martinho da Serra observations was considered the suitable correlation model to be used to create the weather data files for Asunción. The comparison results are depicted through Taylor diagrams, which provide a way of graphically summarising how closely a model matches observations [27].

3.3 Performance metrics - Taylor diagram analysis

The Taylor diagram has been widely used to evaluate climate models over the past years because of its useful features to compare and evaluate multiple aspects of models and gauging the relative skill of many different models [28–31]. Each point in the two-dimensional Taylor diagram can represent simultaneously three statistics (R, RMSD and σ) (see Figures 3-9). The correlation coefficient R is a number between -1 and +1 measuring the strength or consistency of the relationship between two variables (x and y). If R=0 the two variables are uncorrelated. A positive correlation means that x and y vary in the same direction (if x is larger than the $\bar{x}$ mean, then y will also (on average) be larger than the $\bar{y}$ mean). For a negative R, x and y vary

in opposite directions (a larger *x* will imply a smaller *y*). If R=1 then *x* and *y* are completely correlated, indicating a perfectly consistent relationship [32,33]. The centered root-mean-square difference (RMSD), is the most widely used statistic to quantify differences between two variables; as the two variables become more alike, the RMSD approaches zero [34]. The standard deviation σ is the standard distance between the *x* variable and the $\bar{x}$ mean of the dataset and it measures the fluctuations of the error around this mean [33,35]. As the standard deviation of the *x* variable approaches the standard deviation of the *y* variable, the two variables will have the same dispersion and spatial variability. In this way, given a "simulated" field (*f*) and a reference/observed field (*r*), the formulas to calculate these three statistics are described below [27].

$$R = \frac{\frac{1}{N}\sum_{n=1}^{N}(f_n - \bar{f})(r_n - \bar{r})}{\sigma_f \sigma_r} \tag{7}$$

$$RMSD = \frac{1}{N}\sum_{n=1}^{N}\left[(f_n - \bar{f}) - (r_n - \bar{r})\right]^2 \tag{8}$$

$$\sigma_f{}^2 = \frac{1}{N}\sum_{n=1}^{N}(f_n - \bar{f})^2 \tag{9}$$

$$\sigma_n{}^2 = \frac{1}{N}\sum_{n=1}^{N}(r_n - \bar{r})^2 \tag{10}$$

In the Taylor diagram, the RMSD between the simulated and observed patterns is proportional to the distance to the point on the x-axis identified as "REF", which is the reference data. The dashed arcs indicate the RMSD. The standard deviation of the simulated pattern is proportional to the radial distance from the origin (dotted arc). The solid arc indicates the standard deviation of the reference. Simulated or estimated patterns that agree well with observations will lie nearest the point marked "REF" on the x-axis. These models will have a relatively high correlation (dot-dash line) and low RMS errors. Models lying on the solid arc will have the correct standard deviation (which indicates that the pattern variations are of the right amplitude) [27].

As indicated in the next section of the present work, all the datasets herein considered were arranged on a 3hs-time frequency in order to standardise the time steps and make the parameters and statistics comparable. The evaluation was based on annual and seasonal datasets, aiming to analyse the accuracy of the models according to the seasons. Seasons are defined according to the astronomical seasons in Paraguay: spring from 21/09 to 20/12, summer from 21/12 to 20/03, autumn from 21/03 to 20/06 and winter from 21/06 to 20/09. In addition, the normalised diagram is used to analyse various climate parameters and depict them in the same plot. For this purpose, the units of variables were removed dividing both the RMSD and the standard deviation of the simulated/estimated field by the standard deviation of the observations. In this case, the "reference" point is plotted on the x-axis at unit distance from the origin.

3.4 Creation of weather files for energy simulations

Finally, weather data files for energy building simulations were created for each dataset obtained from the regional climate models for Asunción by using the Elements-Big Ladder Software [36]. It is important to underline that the year 2009 was chosen because it was the only year for which it was possible to obtain complete and valid yearly weather datasets from all the sources herein considered (CORDEX, MM5 and above all, the real data from the Silvio Pettirossi Airport).

3.5 Evaluation of energy performances of a building in Asunción using different weather data files

The final step was to model a historical residential building using DesignBuilder Software to evaluate its energy performance according to each weather data file. The building, representative of the historical residential typology in the centre of Asuncion, was analysed both in its original state and in an energy efficient version, to assess the sensitivity concerning the different generated input weather data files. Comparisons were carried out in terms of discomfort rates by considering two methods: the former (in accordance with the acceptable indoor operative temperatures for buildings in Category II of the standard EN 15251 for the design of buildings without mechanical cooling systems) [37] which employs the adaptive method [38]; and the latter, applying the statistic method using fixed threshold values of comfort temperature. This approach was already adopted for the thermal comfort assessment of buildings through various scientific research [39–44].

In order to set the fixed range for the city of Asunción which does not have a national standard energy code, a scientific literature analysis was performed. The static models usually set fixed threshold values of comfort temperatures, and they have been widely used in a significant number of thermal regulations around the world. In Portugal, the thermal regulation sets as acceptable temperatures the range between 18-25°C [45]. In Chile, the Sustainable Construction Code considers acceptable the temperatures between the range of 18-26°C [46]. In Brazil, the NBR 16401-2 [47] sets as acceptable temperatures the range between 23-26°C in the summer season with a relative humidity of 35%. The Chartered Institution of Building Services Engineers (CIBSE) [48] recommends a benchmark summer peak temperature of 28°C for dwelling living areas. In addition, several scientific investigations have been developed to set threshold values of comfort temperature considering the climate under analysis.

Lu et al. [49] developed a field study of thermal comfort in non-air-conditioned buildings in a tropical island climate in China. The results suggest the acceptable temperature range of thermal comfort for the residents was from 23.1 °C to 29.1 °C. Djamila et al. [50] explored the thermal perceptions of people in the humid tropics of Malaysia employing different thermal perception approaches; the results suggest that the optimum temperature was found to be about 30°C. Perhaps the only work assessing thermal comfort conditions (by taking Paraguay as case study) was developed by Lopez et al. [51], for which three naturally-ventilated buildings in Asunción were evaluated, and the results were compared to three different methodologies. The outcomes of the research proved that heat discomfort was overestimated by the ISO 7730 standard when air temperature values exceeded 30 °C since users reported neutral thermal conditions, while the method indicated intense heat discomfort. Furthermore, it was stated that methods employing equations as a function of the outdoor climate variables could successfully

adjust to the hot-humid climatic context. In this way, it was possible to assert that the occupants of naturally-ventilated buildings have a higher tolerance of high temperatures and greater thermal comfort range. Considering the fixed ranges employed by the reviewed standards and those obtained from scientific researches, the fixed range used for this research was 18°C to 28°C.

Annual and weekly indoor air temperature profiles are modelled hourly for the thermal zone presenting the worst thermal performance and, the percentage of the simulated time in which the operative temperatures exceed 28°C or the value recommended by the EN 15251 for buildings in the Category II corresponds to the overheating rate. Similarly, the percentage of the simulated time in which the operative temperatures are lower than 18°C or the value recommended by the EN 15251 for buildings in the Category II corresponds to the underheating rate.

In addition, other simulations were run to analyse the impact of the different climate files considering building profiles of heating and cooling energy needs. These analyses aim to calculate the amount of sensible energy that must be removed or supplied, during the summer or winter season respectively, in order to ensure comfortable indoor conditions. For a better estimation, two different simulation periods are considered: the annual and the weekly simulation.

4. Weather data sources

This section describes the different sources used in this research to create the six weather datasets under analysis. Observed data collected from a weather station for the city of Asunción and São Martinho da Serra were compared to simulated values, obtained from four different regional climate models, and to the typical averaged weather data file of IWEC. In addition, a methodology for the estimation of global solar radiation values is presented in subsection 4.5, coupled with the description of five different correlation models to decompose the global solar radiation value into its diffused and direct components, which are also evaluated through a statistic comparison of the estimated values with observed data collected for the city of São Martinho da Serra.

4.1 Observed meteorological data

This research uses as reference the observed meteorological data of two cities. The collected data refer to the year 2009, which was not a particular cold or hot year since it did not present extreme weather conditions when compared to the records available from 2001 to 2011; it was selected for the analysis because it was the only year for which the percentage of valid data was about 100%.

Regarding temperature, atmospheric pressure, relative humidity, wind speed, wind direction and cloud cover, the collected data comes from the Meteorology Department of the National Direction of Civil Aeronautics of Paraguay (DINAC, by their Spanish initials), and corresponds to 5 minute interval recordings from 1st January to 31st December 2009. The weather station is in the Silvio Pettirossi Airport of Asunción at 25°14' Southern latitude, 57°30' Western longitude and 83 meters above the sea level. In regards to the climate, the annual average temperature in Paraguay is 24°C. The country has springs and winters

9

with pleasant temperatures, generally without frost with average temperatures of 19 °C. Summers are sweltering with a high percentage of humidity, and in some regions including Asunción the temperature may exceed 41°C [52]. According to the climate classification system developed by Köppen-Geiger [53], Asunción has a humid subtropical climate denominated **Cfa**. The **C** group corresponds to "Warm Temperate" climates, the small letter **f** means "fully humid" and indicates the lack of a dry season and the letter **a** corresponds to a "hot summer".

For global, diffused and direct solar radiation, the data collected in 2009 was observed from a weather station in São Martinho da Serra, located at 29°26' Southern latitude, 53°49' Western longitude and 489 meters above the sea level. The source corresponds to the Brazilian Environmental Data Organization System (SONDA, by their Portuguese initials), an initiative of the National Institute for Space Research (INPE, by their Portuguese initials), which has several stations around the country measuring the three irradiance components on a minute basis [26]. According to the Köppen-Geiger classification, also this city is under the **Cfa** zone [53]. The mean maximum air temperature is 24 °C and the mean minimum temperature is 14 °C [26].

4.2 Fifth Mesoscale Model

MM5 is the PSU/NCAR Mesoscale Model Fifth Generation (MM5), developed by the Penn State University (PSU) and the National Center for Atmospheric Research (NCAR) and it is a model system able to simulate or predict mesoscale and regional-scale atmospheric circulation. Initially, this model was only hydrostatic, but after some further releases it has definitively become non-hydrostatic. It is based on the momentum and energy conservation equations and adopts a tendency equation for the perturbation pressure (model prognostic on the pressure variable). The model employs a σ pressure coordinate system, based on the hydrostatic pressure reference, and uses finite difference numerical schemes (Arakawa B staggering). Further information can be found in Grell et al. [54] and Dudhia et al. [55].

In this work, the simulating features of the MM5's surface meteorological parameters were statistically evaluated using two different combinations of planetary boundary layer (PBL) and land surface model (LSM) parameterisation schemes. The first one corresponds to the PBL of Medium Range Forecast model (MRF) developed by Hong & Pan [56] combined with the NOAH LSM (hereafter referred as MM5-MRF-NOAH). The second combination comprises the PBL developed by Pleim & Chang [57] combined with the LSM developed by Pleim & Xiu [58] (hereafter referred as MM5-PLEIM-XIU).

Annual climate reconstructions were performed by using a hindcasting procedure with the MM5v3.7 model. The output area of interest represents the fifth domain of a 2-way nesting procedure; in this way, all meteorological phenomena, from synoptic to local, was considered with the correct spatial resolution and finer and coarser results are shared among different levels at every time step. The used input met database is the NCEP archive (National Centers for Environmental Prediction) ds083.2, which belong to Final Global Data Assimilation System (FNL) category. These data are classified as global tropospheric analyses and come from all around the world (met station, wind masts, ships, met balloons and so on). FNL data are the basis of the global

forecasting system and are carried out using a high definition model; ds083.2 data are available from 1999 to present day with a grid of 1°x1° resolution and 52 vertical levels. Each ds083.2 file contains 286 data covering a period of 4 hours. Vertical levels (named sigma levels) cover a range from 1000 [hPa] down to 10 [hPa]. Analyses are stored four times a day (00:00, 06:00, 12:00, 18:00 UTC) and contain information for 6 hours. Land use database is the USGS version 2 that allows operating with a resolution of 30 arcseconds (~ 1 km).

The collection of datasets for Asunción used simulations which covered a 1-year period from 1st January 2009 to 31st December 2009; the adopted hindcasting procedure created a virtual meteorological mast placed in the same position of the real mast and featuring output values with 4-minute interval and measurement plans from 10-meters up to 500 m above surface. The inner model domain, centered in the Silvio Pettirossi Airport, was 33x33 km wide and had a grid spacing of 1 km. The integration domain covered Asunción from 14° to 45° S to 70° to 37° W. For São Martinho da Serra, the simulations covered the same year period and provided a virtual meteorological mast in the same position as the real one. In addition, in this case, the inner domain model was 33x33 Km wide, and it had a grid spacing of 1 km. The outer integration domain covered an area from 18° to 40° S and from 67° to 41°W. Through these simulations, it was possible to obtain simulated values for the meteorological parameters regarding temperature, atmospheric pressure, relative humidity, wind speed, wind direction and global solar radiation. Hence, to create the weather data file for the energy simulations, the estimation of the diffused and direct components of solar radiation was developed starting from the global radiation value and according to the best correlation model obtained in section 3.2 of this research.

4.3 Coordinated Regional Climate Downscaling Experiment

CORDEX is a project aiming to develop a coordinated framework for evaluating and improving Regional Climate Downscaling (RCD) techniques and producing a new generation of RCD-based fine-scale climate projections for identified regions worldwide [59]. For the South American CORDEX domain and data generated with a 3hs-time frequency for the year 2009, the project has two regional climate models available. The first one corresponds to the HadRM3P developed by the Meteorological Office Hadley Centre (MOHC), which operates on a rotated longitude-latitude grid with 0.44° resolution in both horizontal directions and 19 levels in vertical [60]. The second regional climate model corresponds to the fourth version of the Rossby Centre Regional Atmospheric Climate Model (RCA4) developed by the Swedish Meteorological and Hydrological Institute (SMHI), which operates on a rotated longitude-latitude grid of 0.11° and 0.44° horizontal resolution and 40 vertical levels [61]. Both regional models use the ERA-Interim global driving model, a global atmospheric reanalysis with a spatial resolution of the data set of approximately 80 km and 60 vertical levels from the surface up to 0.1 hPa, which was developed by the European Centre for Medium-Range Weather Forecasts (ECMWF) [62]. The meteorological parameters available with the HadRM3P model are temperature, atmospheric pressure, specific humidity, wind speed, cloud cover and global solar radiation. For the RCA4 model, the same parameters are available but excludes cloud cover.

One dataset for each regional climate model was drawn from the nearest grid point to Asunción, which is 25°11' Southern latitude, 57°51' Western longitude: 13.54 km away from the airport meteorological mast. In addition, datasets from the nearest grid point to São Martinho da Serra were extracted, located 29°51' Southern latitude, 54°07' Western longitude, 24.94 km away from the meteorological mast. The weather datasets also refer to 2009, and the values for the components of solar radiation were also estimated from the values obtained for global solar radiation.

Finally, it is important to clarify that in order to get hourly data for the climate parameters under study, a cubic spline function was used to attain interpolated values by checking the physical representativeness of the obtained trends.

4.4 International Weather for Energy Calculations (IWEC)

DesignBuilder (DB) uses Energy Plus format hourly weather data (.epw) to define external conditions during simulations. Each location has a separate file describing the external weather conditions for every hour of the year at that location. These hourly weather data are 'typical' data derived from hourly observations. Many of these weather files correspond to a record of multiple years, where each selected month is representative of that month for the period of record; the data is representative of the normal patterns for that month and is not intended to be the average. The selection of months is usually based on a weighing of temperature, humidity, wind, and solar radiation [63].

The weather datasets used for this work correspond to the default weather file available in DB for Asunción, which has hourly weather data obtained from the International Weather for Energy Calculations [64]. The weather station corresponds to the Silvio Pettirossi Airport, and the dataset was obtained over an 18-year period (1982-1999 for most stations). As this weather data source may represent the most used source for building energy simulations, it was included in the present analysis to determine its reliability against single year weather data, considering that for the calibration of building energy models, the real energy consumption data, normally cover a specific period of time (monthly or annual), and do not represent averaged values of multiples years. Table 1 summarises the weather datasets used in the present analysis, reporting the name and a brief description of the data source for each climatic file.

Table 1 - Weather datasets used in this research.

Weather dataset	Description
Observed – 2009	Dataset for the year 2009, collected from a weather station in Asunción and São Martinho da Serra
CORDEX-HadR3mP	Dataset for the year 2009, extracted with the HadRM3P regional model developed by MOHC
CORDEX-RCA4	Dataset for the year 2009, extracted with the RCA4 regional model developed by SMHI
MM5-MRF-NOAH	Dataset for the year 2009, extracted with the MRF PBL developed by Hong & Pan, combined with the NOAH LSM
MM5-PLEIM-XIU	Dataset for the year 2009, extracted with the PBL developed by Pleim & Chang, combined with the LSM developed by Pleim & Xiu
DB-IWEC	Default dataset available in DB for Asunción obtained from IWEC

4.5 Estimation of Global Solar radiation and its diffused and direct components

Several scientific investigations have developed and analysed different models to estimate global solar radiation and its diffused and direct components [65–73]. Comprehensive reviews of these models can be found in [74,75]. The model used in the present paper estimated the hourly global solar radiation and used as input parameters the temperature (T [°C]), atmospheric pressure (P [kPa]) and relative humidity (RH [%]). The first step was to calculate the optical air mass number (m [-]), which expresses the ratio of slant path length through the atmosphere to zenith path length [76] according to equation (1),

$$m = \frac{P/P_o}{\sin\alpha_s + 0.50572 \times (\alpha_s + 6.07995)^{-1.6364}} \tag{1}$$

where P_o[kPa] is the atmospheric pressure at sea level and α_s [°] is the solar altitude angle of the sun. The expression to calculate α_s can be found in [77]. The second step was to determine the atmospheric transmittance coefficient (τ [-]). Beam atmospheric transmittance is the percentage of the beam (direct) radiation that will penetrate the atmosphere without being scattered [78]. For τ values lower than about 0.4 overcast sky would be considered, and for the clearest days the value would be around 0.75 [76]. For this work, in order to calculate τ value the decision matrix developed by Al Riza et al. [78] was considered, which is based on the method developed by Spokas & Forcella [79], and considering the concept that water vapour by means of relative humidity (RH) reduces incoming radiation. Thus, the authors created a decision matrix to determine τ by using measured RH. The decision matrix is shown in Table 2. In addition, in each case, the range regarding daily extreme temperatures (ΔT) must be checked to assure it is less than 8°C. Thus, if $\Delta T < 8°C$, $\tau' = \frac{\tau}{(11 - \Delta T)}$ (2)

Table 2 - Decision matrix to determine atmospheric transmittance [78]

N°	RH condition (%)	τ value
1	RH≤40	0.69
2	40<RH≤45	0.67
3	45<RH≤55	0.57
4	55<RH≤65	0.47
5	65<RH≤75	0.41
6	75<RH≤80	0.30
7	RH>80	0.20

At this point, it is possible to calculate the direct radiation on a surface perpendicular to the beam (I_p [$W \cdot m^{-2}$]), which is a function of global solar constant ($G_{sc} = 1367\ W \cdot m^{-2}$) and the optical air mass number (m) (Equation 3); in addition to calculating the direct radiation on a horizontal surface (I_{dir} [$W \cdot m^{-2}$]) (Equation 4) and the diffused radiation on a horizontal surface (I_{diff} [$W \cdot m^{-2}$]) (Equation 5), which are a function of the zenith angle of the sun (θ_z). Finally, global solar radiation (I_{gl} [$W \cdot m^{-2}$]) can be calculated from Equation 6 [76].

$$I_p = G_{sc} \times \tau^m \tag{3}$$

$$I_{dir} = I_p \times \cos\theta_z \tag{4}$$

$$I_{diff} = 0.30(1 - \tau^m) \times G_{sc} \times \cos\theta_z \tag{5}$$

$$I_{gl} = I_{dir} + I_{diff} \tag{6}$$

This methodology is a simple model based on Liu & Jordan [80], developed and suggested by Campbell & Norman [76] (hereafter just referred as Campbell & Norman). The previous methodology was used to estimate global solar radiation values and its components, to solve the problem of missing data for the reference weather data file. However, for the MM5 and CORDEX weather files, the values of global solar radiation are available. Thus, to estimate the values of their diffused and direct component, correlation models which use global solar radiation and clearness index as input parameters were implemented.

Many investigations have estimated the components of global solar radiation by considering the approach of correlating I_{diff}/I_{gl} (the fraction of the hourly radiation on a horizontal plane which is diffused) with k_t, the hourly clearness index [81]. A review of the different models can be found in [82]. To determine the diffused fraction (I_{diff}/I_{gl}) using the models here described, a calculation was required of the hourly clearness index k_t by means of the ratio referred by Liu & Jordan [80], $k_t = I_{gl}/I_{ext}$, where I_{ext} is the hourly extra-terrestrial radiation on the horizontal surface (referred to as the radiation above the earth's atmosphere). The formula to calculate it can be found in [77].

The widely used correlations correspond to those developed by Erbs et al. [83], Liu & Jordan [80], Orgill & Hollands [84], among others. However, several researchers have also developed different regression analyses to obtain correlations considering the observed data in their countries. Chikh et al. [85] developed correlation models for three cities of Algeria. Marques et al. [86] developed a sigmoid logistic function to represent the relationship between the diffused fraction and the clearness index for Rio de Janeiro, Brazil. The authors concluded that the models perform well when compared with the most widely used models and can be applied to estimate the values of diffused and direct components of global solar radiation. In the same line, Ridley et al. [87] developed a multiple predictor model and concluded that the model performs consistently well in both hemispheres and can be used as a universal model. For the present work, five correlations models were employed.

The Erbs et al. correlation [83],

$$\frac{I_{diff}}{I_{gl}} \begin{cases} 1.0 - 0.09k_t & \text{for } k_t \leq 0.22 \\ 0.9511 - 0.1604k_t + 4.388k_t{}^2 - 16.638k_t{}^3 + 12.336k_t{}^4 & \text{for } 0.22 < k_t \leq 0.80 \\ 0.165 & \text{for } k_t > 0.80 \end{cases}$$

The Orgill & Hollands Correlation [84],

$$\frac{I_{diff}}{I_{gl}} \begin{cases} 1.0 - 0.249k_t & \text{for } k_t \leq 0.35 \\ 1.557 - 1.84k_t & \text{for } 0.35 < k_t \leq 0.75 \end{cases}$$

0.177 $\qquad$ for $k_t > 0.75$

The sigmoid logistic function developed by Marques et al. [86],

$$\frac{I_{diff}}{I_{gl}} = 0.13 + 0.86 \frac{1}{1+exp\left(-6.29+12.26k_t\right)} \qquad \text{for } 0 < k_t \leq 1$$

The BRL model developed by Ridley et al. [87] uses hourly clearness index k_t, daily clearness index K_T, solar altitude $\alpha_s[°]$, apparent solar time AST [h] and a measure of the persistence of solar radiation level ψ [-] as predictors.

$$\frac{I_{diff}}{I_{gl}} = \frac{1}{1+exp\left(-5.38+6.63k_t+0.006AST-0.007\alpha_s+1.75K_T+1.31\psi\right)} \qquad \text{for } 0 < k_t \leq 1$$

In addition to the original BRL model previously referred, an adjusted BRL model for Brazil was developed by Lemos, et al. [88] based on the same set of parameters but adjusting the constant coefficients to achieve better estimations. Aiming to compare both models and considering that one of the cities under analysis is from Brazil, the accuracy of this model was also assessed.

$$\frac{I_{diff}}{I_{gl}} = \frac{1}{1+exp\left(-4.41+7.87k_t-0.088AST-0.00490\alpha_s+1.47K_T+1.10\psi\right)} \qquad \text{for } 0 < k_t \leq 1$$

Figure 2 summarises the methodology applied in this subsection.
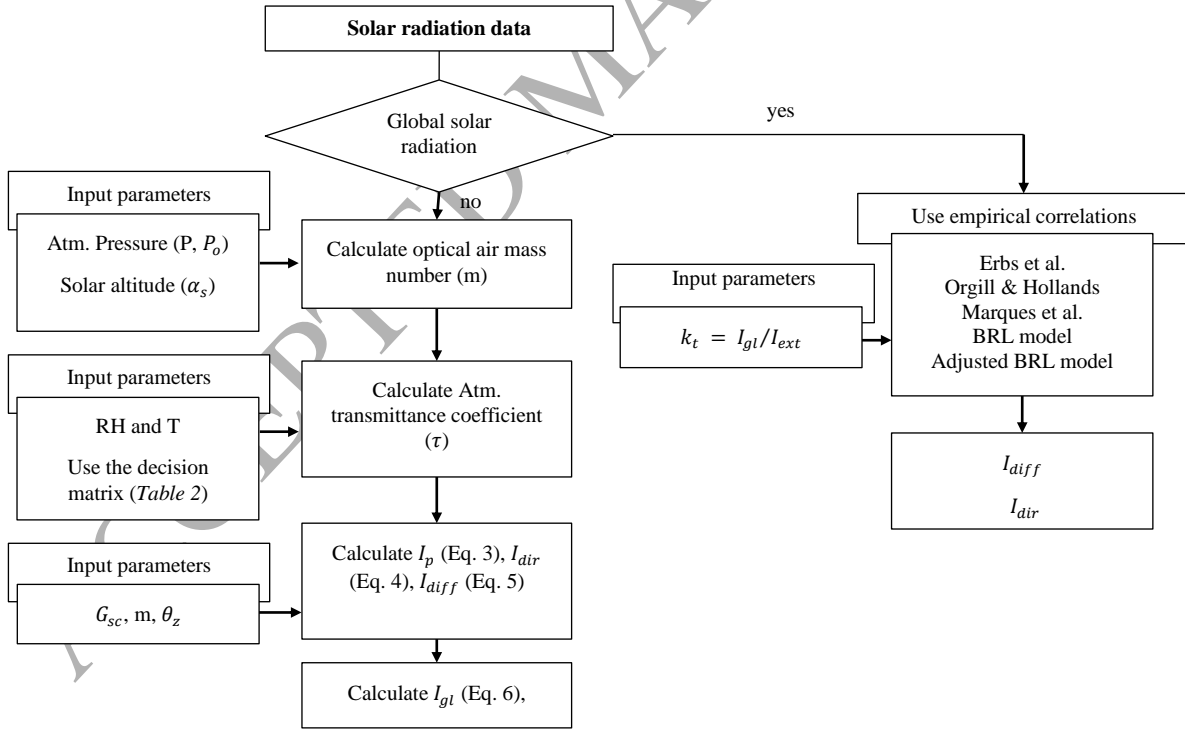
Figure 2 – Methodology for the estimation of global solar radiation and the use of correlation models.

4.5.1 Quality control of data

In the estimation procedure of the diffused and direct components of solar radiation, the values obtained were checked and controlled for errors and irregularities. The purpose of data quality control was to eliminate faulty and inconsistent data. The

first quality control used for the selection of measured data involved the elimination of those values that led to zenith angles greater than 90° since they were considered unphysical values. The second quality control was used for the decomposition of global solar radiation into its direct and diffused components. As suggested by many authors [82,86,88] the set of filters applied are related to the solar altitude angle α_s (α_s >7°), the persistence factor ψ (0< ψ <1), the hourly and daily clearness index (0<k_t; K_T <1) and the diffused fraction d (0< d <1). After applying these filters, the number of hourly values for the comparisons between the correlation models decreased from 8760 to 3956 values.

5. Intercomparison between weather datasets

5.1 Weather datasets for Asunción, Paraguay.

In this section, the general performance of climate models in simulating the surface climatology of Asunción is examined. For the analyses of the model skills, the results are shown based on seasonal (Figure 3) and annual datasets (Figure 4a). In a general approach, it can be seen that the performance of the models varies according to the parameter simulated. In most cases the parameters having lower RMSD and higher correlations are the temperature and the atmospheric pressure (red and yellow markers) since they are located nearest the reference point. The other parameters are scattered throughout the quadrant with most data points within the 1.5 RMSD circle and correlations between 0.2 and 0.6, excluding the datasets of DB which have in most cases the highest RMSD and lowest correlation, and even negative values in some cases (spring and winter season). Regarding the standard deviation, in most cases, the data points fall into the area between the circles of 0.75 and 1.25, indicating that the models can represent the time distribution of the simulated parameters with a good approximation. According to Figures 3a to 3d, the DB (diamond marker) dataset delivered the lowest correlation patterns for all the parameters, being the poorest performance model since its markers are always located the farthest from the reference point.

In the following sections, the results are analysed in depth for each weather dataset, considering each climate parameter under study.

Temperature.

For the temperature parameter (red markers) in the spring season, the data points fall within the 0.75 RMSD circle, excluding the DB data point which has an RMSD= 1.04. The MM5-MRF-NOAH dataset presented lower RMSD and higher correlations (RMSD= 0.53 and R=0.84). Nonetheless, the CORDEX-HadRM3P dataset simulated the amplitude of the variations better than the MM5-MRF-NOAH model (σ=0.96 for the first while σ=0.78 for the second), but with a slightly higher error (RMSD=0.66) and lower correlation (R=0.77). In the summer season, the temperature pattern was similar to that in the spring and with better σ values for the CORDEX datasets but higher RMSD and lower correlation than that obtained with the MM5datasets.

Nonetheless in this season, the model delivering lower RMSD values and higher correlations corresponded to MM5-PLEIM-XIU. Furthermore, the DB dataset performed (statistically) similarly to that of the CORDEX models. In the autumn season, the

16

models performed well regarding the time distribution, delivering values of σ between 0.93 and 1.10, excluding the MM5-PLEIM-XIU dataset which generated little time variability for the temperature parameter in this season (σ=0.75), though it delivered the least errors (RMSD=0.65) and highest correlation (R=0.76). For the winter season, the same pattern was repeated in that the CORDEX datasets simulated the amplitude of the variations better than those of MM5, but this last one delivered the best RMSD and R results. However, the CORDEX-HadRM3P dataset also provided similar RMSD and R values with a σ value equal to 0.91.
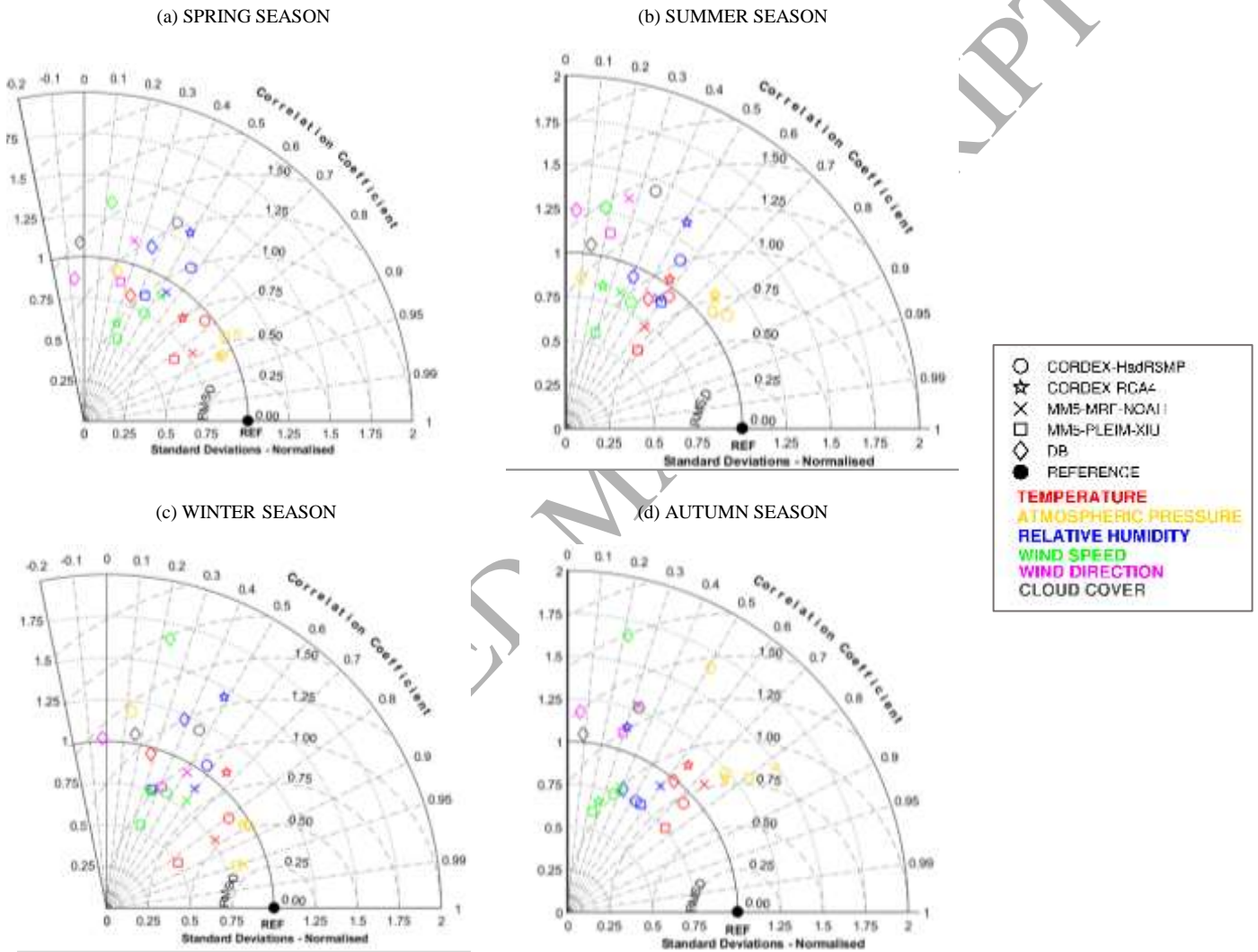
Figure 3 – Normalised Taylor diagrams for (a) Spring season, (b) Summer season, (c) Winter season and (d) Autumn season. Colours indicate the climate parameter and the markers' shape indicate the model under analysis.

Figure 4a depicts the results based on annual datasets, where CORDEX performed well in regards to the time distribution with σ values matching the observations. The MM5 and DB datasets showed a shorter time variability of the parameter with data points falling under the solid black circle (MM5-PLEIM-XIU more than the others with σ= 0.73). Nevertheless, the MM5 datasets delivered lower RMSD values (RMSD= 0.55) and higher correlation values (R=0.84). Very similar values are those obtained by CORDEX-HadRM3P but with better σ values (σ=1.00, RMSD= 0.61 and R=0.81).

A more detailed analysis regarding the temperature parameter was carried out considering the monthly mean temperatures according to the weather data sources under analysis, as depicted in Figure 4b.

In general, the models described the temperature pattern well, reproducing the climatology with a good approximation. Nonetheless, some models performed better in some months than in others. For example, CORDEX-HadRM3P tended to overestimate the temperature mainly in warmer months, and the MM5 datasets underestimated in almost all the months. The DB dataset presented an irregular behaviour, overestimating some months and underestimating others. Thus, considering monthly mean values and excluding three months (March, April and June), the model performing the best corresponds to CORDEX-RCA4, which almost matches observation in the remaining months.

(a) ANNUAL   (b) MONTHLY MEAN TEMPERATURES
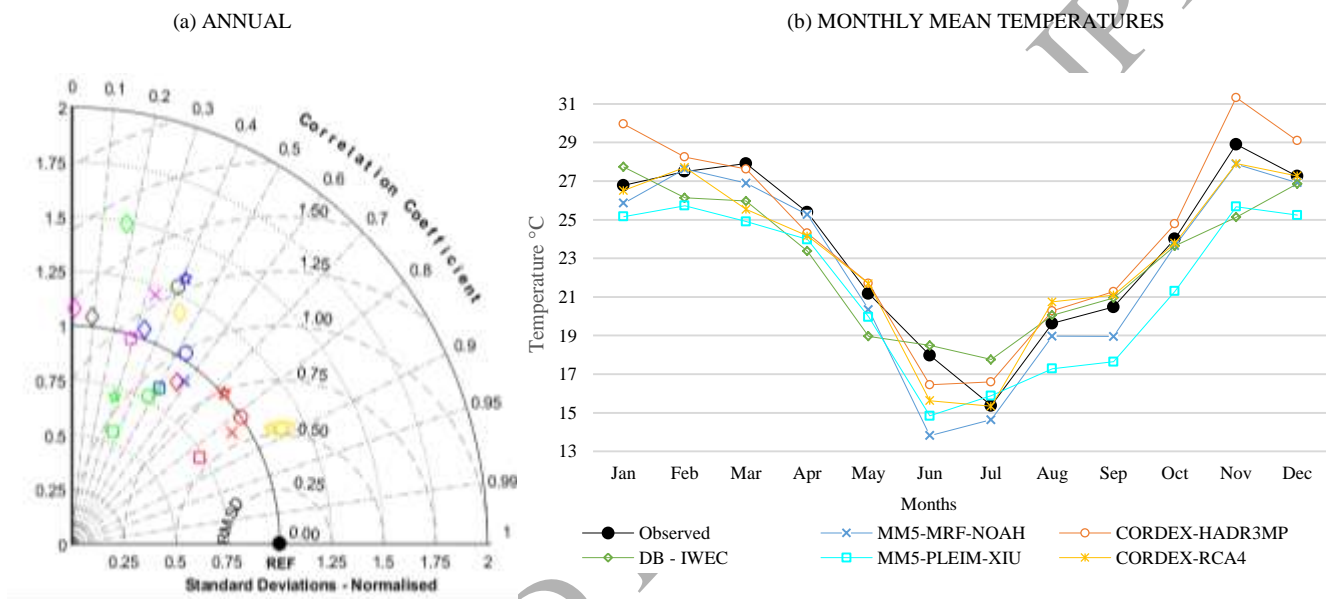
Figure 4 – (a) Normalised Taylor diagram based on annual datasets. (b) Monthly mean temperatures according to the weather data sources under analysis.

Atmospheric pressure.

Considering the results for atmospheric pressure (yellow markers), the CORDEX HadRM3P and RCA4 datasets delivered similar results in each season, presenting the same pattern as MM5. In the spring season, the five datasets performed well in regards to time distribution, delivering σ values between 0.90 and 1.10. The CORDEX datasets delivered slightly lower RMSD and higher correlation than the MM5 datasets (RMSD= 0.43 and R=0.90 for CORDEX against RMSD= 0.54 and R=0.86 for MM5) while the DB dataset was the furthest from the reference point. In the summer and autumn season, the models simulated variations that were much greater than those observed, especially in the autumn season with mean σ values of 1.4, with RMSD values between 0.79-0.87 and correlation values between 0.76-0.82 for CORDEX and MM5 datasets. For the winter season, the MM5datasets showed a shorter time variability (σ=0.84) while the CORDEX datasets performed well regarding the time distribution with σ=0.97. However, the MM5 datasets delivered slightly lower RMSD and higher correlation than the

18

CORDEX datasets (RMSD= 0.32 and R=0.95 for MM5 against RMSD= 0.52 and R=0.85 for CORDEX). For this parameter, the DB dataset always delivered the lowest correlation and the highest RMSD.

Regarding the annual assessment for atmospheric pressure, all the models performed similarly in regards to time distribution, with mean σ values equal to 1.15. Furthermore, excluding the DB dataset, all the models delivered similar RMSD values (≅0.53) and correlations (≅0.88).

Relative humidity.

The blue markers depict the results concerning relative humidity, and for all seasons the correlation values did not exceed 0.60 and the RMSD values did not fall lower than 0.85. The CORDEX-RCA4 dataset tended to simulate greater time variability of the parameter in all seasons with mean σ value around 1.32.

Analysing the annual datasets, the best results can be attributed to the CORDEX-HadRM3P and MM5-MRF-NOAH datasets, which in most of the seasons delivered the highest correlations and lowest RMSD values. The poorest models simulating the relative humidity parameter were the DB and CORDEX-RCA4 datasets, with the highest RMSD values and the lowest correlations. The lowest RMSD values and highest correlations were delivered by the MM5-MRF-NOAH dataset (RMSD= 0.88 and R=0.58) with a σ value equal to 0.92. In regards to time distribution, the best performing model was the CORDEX-HadRM3P (σ=1.03) but with slightly different RMSD and correlations values (RMSD= 0.98 and R=0.53).

Wind speed and direction.

The green markers correspond to the wind speed parameter. Excluding the DB dataset, all the models tended to simulate a small variability of this parameter in all seasons, considering that all the data points fall under the solid black circle which highlights the standard deviation of the observations. Considering the results in terms of wind direction (magenta markers), all the available datasets, MM5-MRF-NOAH, MM5-PLEIM-XIU and DB, delivered high RMSD and low correlation values when compared with observations.

Regarding the annual variability of the wind speed parameter, the furthest dataset from the reference point corresponded to the DB dataset, which simulated a greater time distribution with σ value of 1.50, RMSD equal to 1.64 and correlations of 0.18. The model performing best among the analysed models was the MM5-MRF-NOAH, presenting a σ value of 0.82, RMSD equal to 0.92 and correlations of 0.50. For the wind direction parameter, the MM5-MRF-NOAH model delivered the highest correlation (R=0.33), while the lowest RMSD values were delivered by MM5-PLEIM-XIU (RMSD= 1.18), which also performed well in regards to the time distribution among the three datasets available (σ=0.98).

Cloud cover.

The black markers portray the results concerning cloud cover. For this parameter two datasets were available (CORDEX-HadRM3P and DB) and, as was seen for wind direction, all of them delivered high RMSD and low correlation values when

compared to the observed data for all seasons. Considering the annual datasets, the highest correlation was 0.40 for CORDEX-HadRM3P and RMSD of 1.27 but with a σ value of 1.28. The DB dataset instead performed well concerning the time distribution with a σ value of 1.04 but with higher RMSD and almost zero correlation value (RMSD= 1.38 and R=0.09).

Therefore, considering the intercomparison between hourly values, the DB dataset recorded the poorest statistics for all the parameters. Nonetheless, it is worth noting that the DB dataset did not correspond to simulated or generated weather data for the year 2009, as was developed for the other models, and the datasets were compared with observed data for this specific year. However, the DB dataset corresponded to the weather data file presented in DesignBuilder and Energy plus as typical and representative of Asunción's climate, but when compared with this specific year, the dataset did not perform in agreement with observations. In this way, if real energy consumption data for this year were used for the calibration of building energy models, the DB datasets could affect the results and the datasets obtained from regional climate models would be more recommended.

In general, the model skills for temperature and atmospheric pressure were better than those for the other parameters since most of their data points always clustered near the reference point. The climate models could reproduce the surface climatology of Asunción for the year under study. However, large spreads existed among the models for all the parameters analysed (excluding temperature and atmospheric pressure). The CORDEX datasets tended to perform better in regards to time distribution while those of MM5 had slightly better results in terms of RMSD and correlation values but with a tendency to simulate shorter time variability than observations. Overall, among the analysed models, the models which performed slightly better were CORDEX-HadRM3P and MM5-MRF-NOAH, which tended to behave similarly on an annual basis and statistically, analysing each parameter, they demonstrated slightly better skills in depicting time distribution, RMSD values and correlation values than the other models investigated.

5.2 Weather datasets for São Martinho da Serra, Brazil

This section analyses the general performance of climate and correlation models in simulating/estimating global solar radiation and its direct component for the city of São Martinho da Serra, and the results shown are based on seasonal and annual datasets. Figure 5, Figure 6 and Figure 7 depict the results for the global solar radiation parameter, while Figure 8 and Figure 9 regard the direct component of global solar radiation.

Global solar radiation.

The regional climate models, both MM5 and CORDEX, were in general able to describe the variation of global solar radiation during the seasonal and annual periods. According to Figures 5 and Figure 6, the MM5 datasets (square and x markers) agreed best with observations for all seasons, considering that both MRF-NOAH and PLEIM-XIU are always the closest to the reference point, particularly during the colder seasons. In fact, MM5-MRF-NOAH recorded the lowest distance from the reference in the autumn season, with a 0.43 RMSD value and a correlation equal to 0.91. In the same way, CORDEX was able to describe the time variability of global radiation well during the seasons. Nevertheless, the models delivered slightly lower

correlations and higher RMSD values than those of MM5. When compared to each other, CORDEX-RCA4, which had a lower RMSD (0.50) and higher correlation coefficient (0.87), was more accurate than CORDEX-HadRM3P, which had values equal to 0.51 and 0.86, respectively. The model developed by Campbell & Norman could be useful when measured or simulated data for global solar radiation is unavailable (even if it is not as accurate as the regional climate models). In general, the model tended to estimate variations that were much greater than observations, delivering slightly better results in the warmer seasons, recording its best value in summer (0.67 RMSD value, R=0.86 and σ=1.30) and becoming less accurate in winter (1.09 RMSD circle, R=0.77 and σ=1.65).
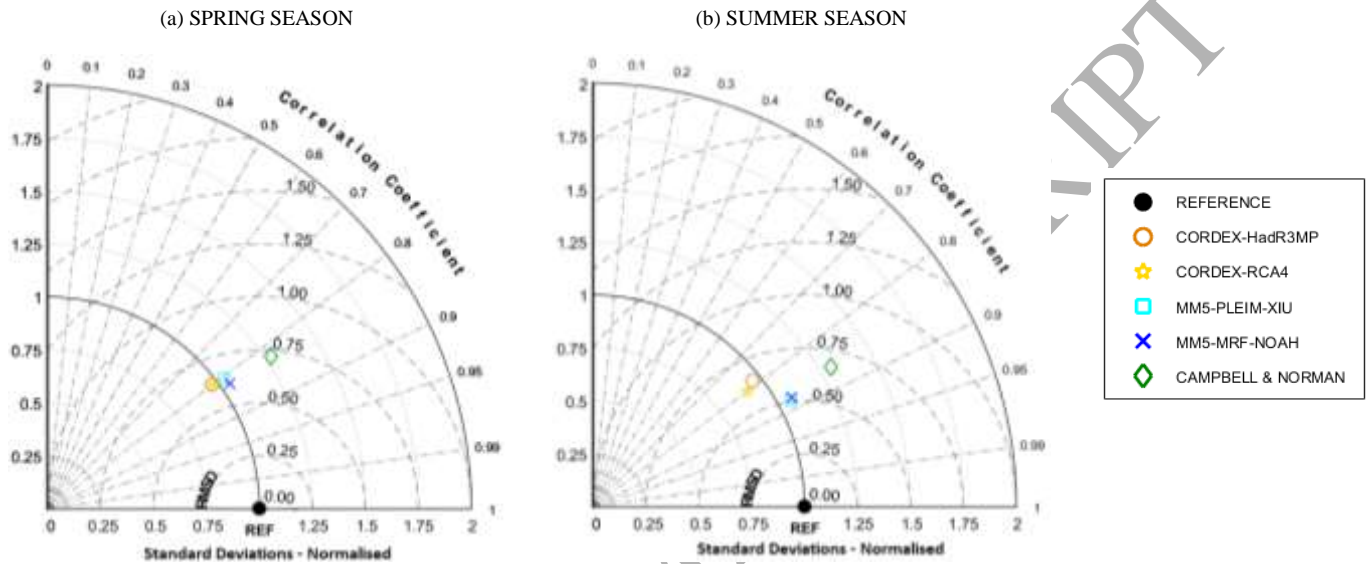
Figure 5 - Normalised Taylor diagrams for (a) Spring season and (b) Summer season, analysing results of Global solar radiation
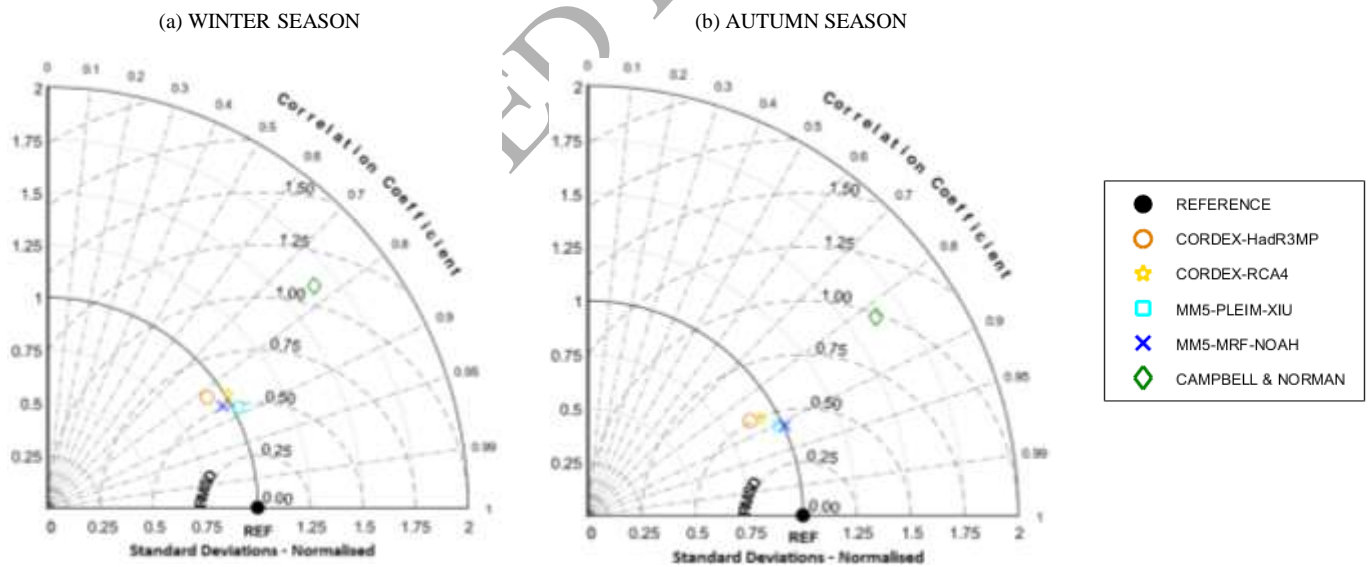
Figure 6 - Normalised Taylor diagrams for (a) Winter season and (b) Autumn season, analysing results of Global solar radiation.

ANNUAL
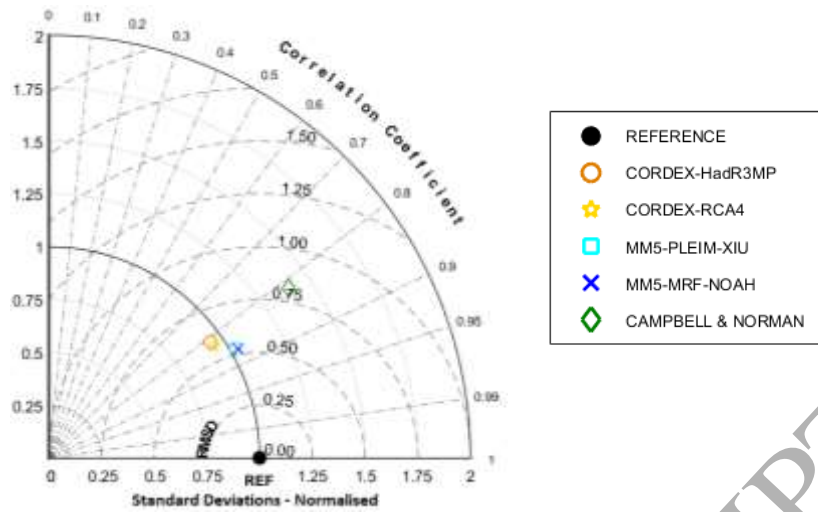
Figure 7 - Normalised Taylor diagram based on annual datasets, analysing results of Global solar radiation.

The trend analysed for seasonal datasets is also confirmed in Figure 7, where the results based on annual datasets are shown. The MM5 models described the global solar radiation for the annual dataset slightly better; MRF-NOAH with a 0.53 RMSD value and correlation equal to 0.87 and PLEIM-XIU with a 0.54 RMSD value and 0.86 correlation. CORDEX models delivered slightly lower correlation and higher RMSD values. Campbell and Norman's model improved its accuracy when considering the annual dataset, with values of RMSD, R and σ equal to 0.82, 0.82 and 1.39, respectively.

Direct component of solar radiation.

Figures 8 and Figure 9 depict the accuracy of different empirical correlation models to estimate the direct component of solar radiation using the global solar radiation value as input data. Figure 8 shows the results on the seasonal dataset, while Figure 9 depicts the results based on the annual dataset. In general, the correlation models estimated very short time variability of the parameter, especially during the colder seasons, where the markers fall further from the reference point ($\sigma \cong 0.43$ for colder seasons and $\sigma \cong 0.82$ for warmer seasons). Regarding correlation coefficients, the values for spring and summer season were always lower than 0.70, while for the winter and autumn season, the values decreased to 0.40 for all empirical models. The correlation model delivering the best results in all seasons corresponded to the one suggested by Marques et al. [86], which had RMSD and correlation coefficients equal to 0.83 and 0.64 for spring, 0.82 and 0.62 for summer, 0.98 and 0.30 for autumn and 0.95 and 0.35 for winter, respectively.

In Figure 8, the adjusted BRL model and the original one delivered very similar results, and the adjusted BRL model was able to describe the variation of direct solar radiation slightly better than the original one. In fact, the adjusted BRL model had a slightly higher correlation coefficient in every season, especially for spring and winter seasons. Analysing the results based on an annual dataset (Figure 9) the same trend in the seasonal case was observed. The correlation model estimating the direct component of solar radiation slightly better was the one developed by Marques, et al., delivering values of RMSD, R and σ equal to 0.90, 0.52 and 0.81, respectively.

22

In conclusion, the analyses carried out in this section show the accuracy of regional climate models (MM5 and CORDEX) in estimating global solar radiation values. Thus, the regional climate models driven by reanalysis data might be an option when measured data for global solar radiation is unavailable. The results also underline that the estimation of this parameter using the model defined by Campbell & Norman, which considers the observed data of temperature, atmospheric pressure and relative humidity, but is not as accurate as MM5 and CORDEX regional climate models. In regards to the analysis of empirical models for the decomposition of global solar radiation, measured or just estimated into its direct component, in general all the correlation models delivered similar results. The correlation model developed by Marques et al. was slightly better at describing the time variability of the parameter during the seasons and the whole year, recording slightly higher correlation coefficients. For this reason, it was employed to determine the direct and diffused components of solar radiation to create the weather data files used in the energy simulations, as described in the next sections.
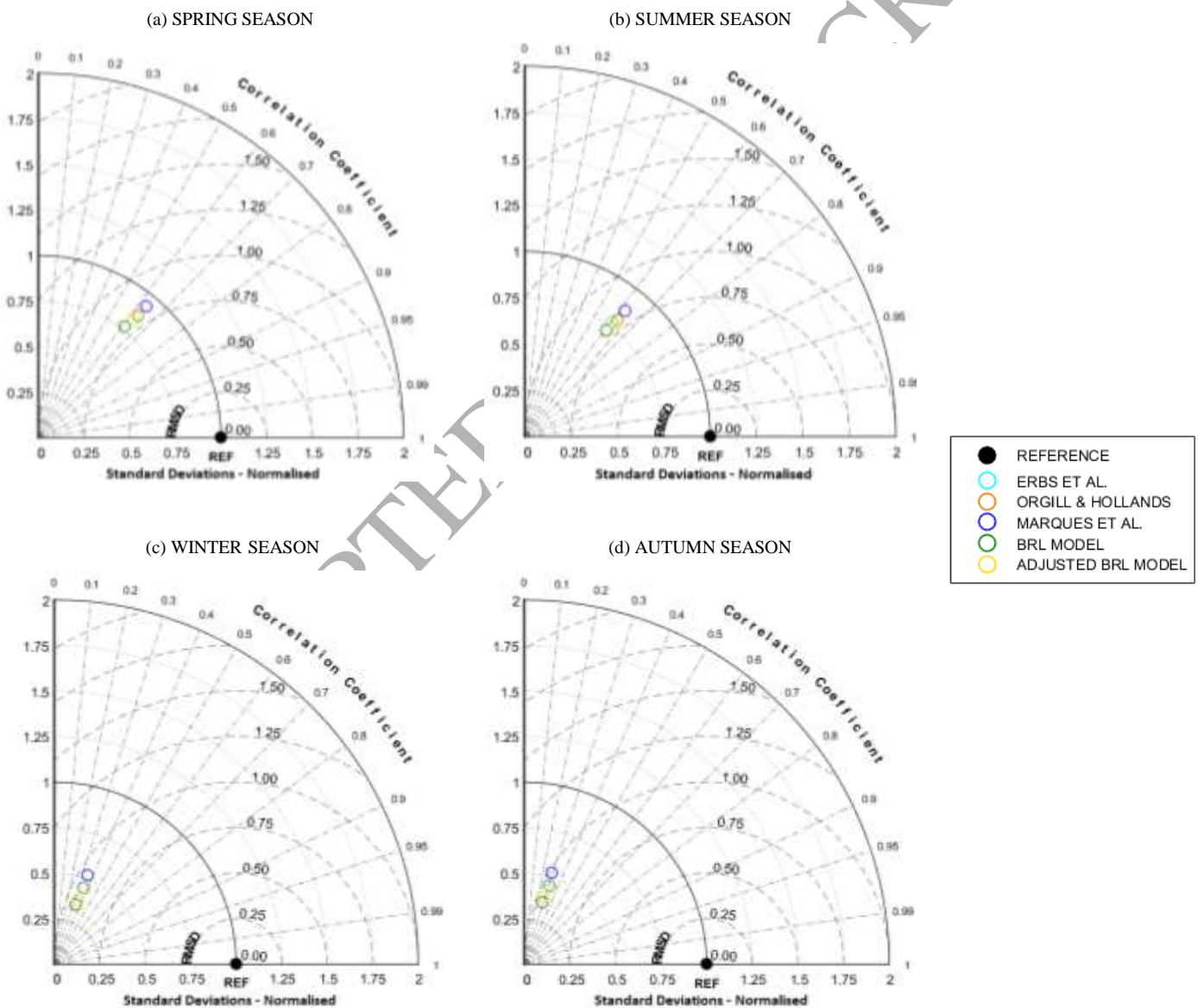
Figure 8 - Normalised Taylor diagrams for (a) Spring season, (b) Summer season, (c) Winter season and (d) Autumn season, analysing results of direct solar radiation. Colours indicate the empirical model under analysis.
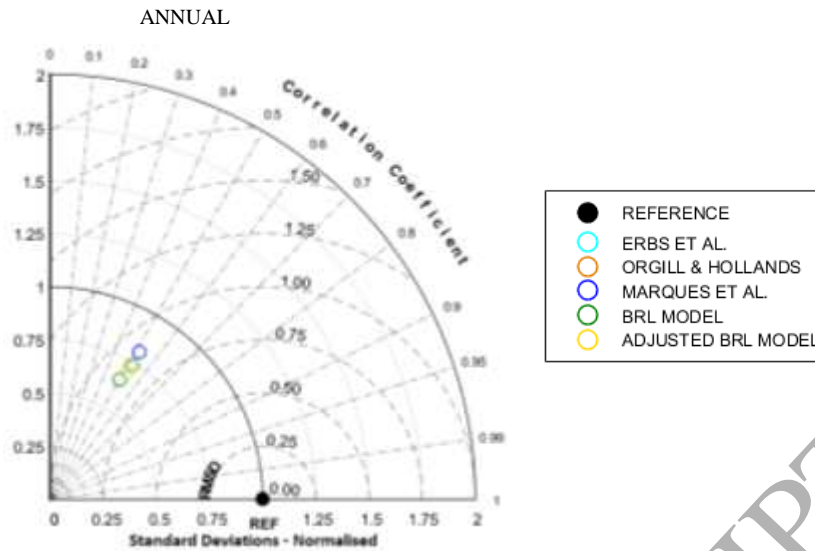
ANNUAL

Figure 9 - Normalised Taylor diagram based on annual datasets, analysing results of direct solar radiation.

6. Building energy performance simulations

6.1 Configuration of simulations

The building under study consists of a historical building located in the Historic Centre of Asunción (CHA, by its Spanish initials). According to a statistical analysis [89], most of the buildings located in the CHA correspond to buildings originally built for residential use (most of them currently abandoned). Almost 60% of residential buildings in the CHA have an Italianate architectural style and were constructed between 1880 and 1930. The case study herein analysed is a residential building with the referred architecture style, representative of most of the CHA's residential buildings, for which it was possible to characterise the building envelope components and materials employed.

The building consists of a two-storey structure and, according to their area and geometry, correspond to a single-family dwelling. The ground floor is composed of four thermal zones (lounge, circulations, bathroom, dining room and a kitchen) and the first floor has three thermal zones (two bedrooms and one lounge) (see Figure 10). The main thermal zone under analysis and for which the results are depicted corresponds to Bedroom 1, a thermal zone on the first floor with an east orientation. The zone was chosen because, considering its exposition and orientation, it records the worst comfort conditions and the highest energy demand.

First, the building was simulated in its original state with the six weather data files which had been previously created. Subsequently, an energy efficient version of the building was also simulated to determine how the different weather files influence the outputs of energy performance. Table 3 summarises the thermal properties of the building's envelope in the original state and the improved solutions. For the dynamic simulations, the metabolic factor is 1 for all thermal zones, as well as the values used for clothing insulations: 0.5 clo for the summer season and 1 clo for the winter season. Table 4 depicts the input parameter values varying according to each thermal zone.
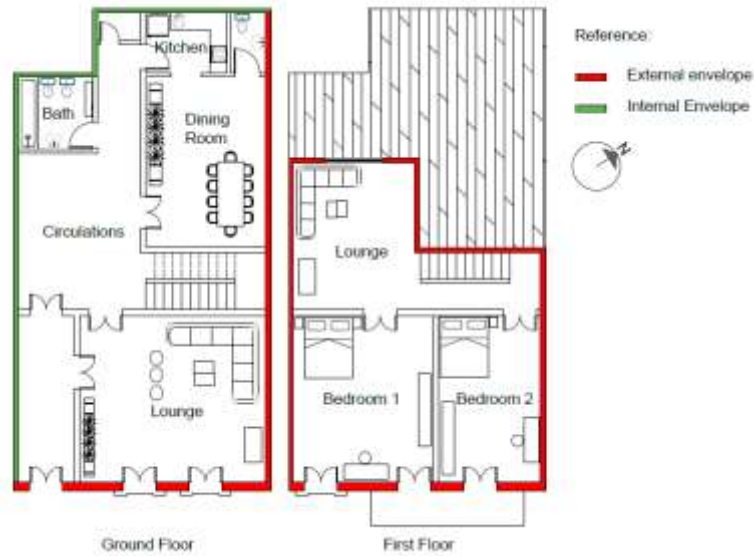
Ground Floor   First Floor

Reference:
External envelope
Internal Envelope

Figure 10 - Case Study architectural blueprints and thermal envelope definition.

Table 3 - Description of the building's envelope components in the original state. For each layer, the values of s (thickness), λ (thermal conductivity), c (specific heat), ρ (density), U (thermal transmittance) and M_s (thermal mass) are shown.

Building component	Material [outer to inner]	s $[m]$	λ $\left[\frac{W}{m\,K}\right]$	c $\left[\frac{J}{Kg\,K}\right]$	ρ $\left[\frac{Kg}{m^3}\right]$	U $\left[\frac{W}{m^2\,K}\right]$	M_s $\left[\frac{Kg}{m^2}\right]$
Configurations in the Original State							
W1- Façade SE orientation 30cm Wall Outer / Inner **(a)(b)(c)**	(a) Sand-lime plaster	0.015	1.15	1000	1800		
	(b) Solid Brick Burned	0.270	0.85	840	1500	1.95	459
	(c) Sand-lime plaster	0.015	1.15	1000	1800		
W2 - NE orientation 20cm Wall Outer / Inner **(a)(b)(c)**	(a) Sand-lime plaster	0.015	1.15	1000	1800		
	(b) Solid Brick Burned	0.170	0.85	840	1500	2.53	309
	(c) Sand-lime plaster	0.015	1.15	1000	1800		
W3 – NE, NW and SW 15cm Wall Outer / Inner **(a)(b)(c)**	(a) Sand-lime plaster	0.015	1.15	1000	1800		
	(b) Solid Brick Burned	0.120	0.85	840	1500	2.93	234
	(c) Sand-lime plaster	0.015	1.15	1000	1800		
F1 - Calcareous Floor	(a) Calcareous tile	0.010	2.21	840	2550		
	(b) Soil-sand screed	0.015	1.15	1000	1800	2.92	277
	(c) Granular subbase	0.100	1.80	840	2240		
R1 - Pitched Roof Tile	(a) High density wood	0.025	0.29	1340	850	4.20	40
	(b) Ceramic Clay Tile	0.010	0.84	800	1900		
G1 - Glazing **(a)**	(a) Single Clear glazing	0.006	0.90	880	2500	5.78	5
Configurations of the energy efficient version [1] [2]							

---

[1] To calculate the thermal parameters of the R1a roof, an equivalent constant thickness was used for the air gap.

[2] For some constructive elements their thermal resistance (R_t) was considered instead of their thermal conductivity.

25
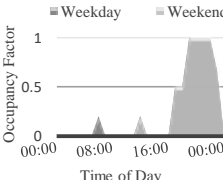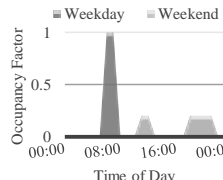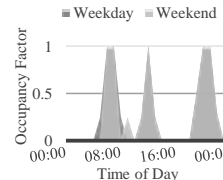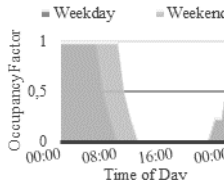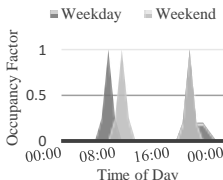
Building component	Material [outer to inner]	s [m]	λ $\left[\frac{W}{m\,K}\right]$	c $\left[\frac{J}{Kg\,K}\right]$	ρ $\left[\frac{Kg}{m^3}\right]$	U $\left[\frac{W}{m^2\,K}\right]$	M_s $\left[\frac{Kg}{m^2}\right]$
W2a - NE orientation 29.5cm Wall Outer — Inner (a) (b) (c) (d) (e)	(a) Thin clay plaster	0.015	0.35	2100	3000		
	(b) Glass wool felt	0.080	R_t= 1.80	840	175		
	(c) Sand-lime plaster	0.015	1.15	1000	1800	0.45	368
	(b) Solid brick burned	0.170	0.85	840	1500		
	(e) Sand-lime plaster	0.015	1.15	1000	1800		
W3a – NE, NW and SW 24.5cm Wall Outer — Inner (a) (b) (c) (d) (e)	(a) Thin clay plaster	0.015	0.35	2100	3000		
	(b) Glass wool felt	0.080	R_t= 1.80	840	175		
	(c) Sand-lime plaster	0.015	1.15	1000	1800	0.46	293
	(b) Solid brick burned	0.120	0.85	840	1500		
	(e) Sand-lime plaster	0.015	1.15	1000	1800		
R1a - Pitched Roof Tile	(a) Ceramic clay tile	0.010	0.84	800	1900		
	(b) High density wood	0.025	0.29	1340	850		
	(c) Air gap	1.000	R_t= 0.15	1000	1200	0.43	1281
	(d) Glass wool felt	0.080	R_t= 1.80	840	175		
	(e) Plasterboard	0.030	0.25	1000	900		
G1a – Double Glazing Outer — Inner (a)(b)(c)	(a) Single clear glazing	0.006	0.90	2500	880		
	(b) Air gap	0.010	R_t= 0.15	1000	1200	2.76	10
	(c) Single clear glazing	0.006	0.90	2500	880		

Table 4 - Input parameters used for the simulations. For each thermal zone the Occupation density (m^2/person), the minimum fresh air (l/s-person), the target illuminance (Lux), the internal gains (W/m^2) and the occupation schedules are shown.

Thermal Zone	Lounge	Circulations	Kitchen & Dining	Bedroom	Bathroom
Occupation	53.32	64.50	59.12	43.59	53.37
Fresh Air	4	4	14	4	10
Illuminance	200	100	300	100	150
Internal Gains	3.90	1.57	30.28	3.58	1.67
Schedule					

For the thermal comfort evaluation, it was taken into consideration that the building does not have any heating or cooling systems. However, natural ventilation was considered, being the natural ventilation rate set in 5 air changes per hour. The window operation schedule defines the operation of natural ventilation. Thus, in the summer season, windows are open and allow natural ventilation only when the outdoor temperature is lower than indoor temperature, but it is restricted when the outdoor temperature is lower than 20°C. In the winter season, windows are open only when the operative temperature is higher than the comfort temperature calculated from the CEN 15251 adaptive comfort model [37], considering that in some winter days the temperature can reach high values. Regarding window shading (exterior Venetian blinds), the schedule concerning aperture operations for the winter season is: 100% open from 8 am to 6 pm and fully closed the rest of the day; for the summer season, windows are shaded when solar radiation on the window reaches the medium solar setpoint of 189 W/m^2 [90], aiming to reduce thermal discomfort due to direct solar radiation but taking advantage of natural daylight.

6.2 Dynamic building energy simulations - Results and Discussions

Once all the weather data files were created and all the input parameters were established, the dynamic energy simulations of the building were carried out. Figure 11 and Figure 12 depicts the results of the annual thermal comfort evaluation, while Figure 13 shows the annual energy requirements of the thermal zone under analysis, using the different climatic files and considering both, the original state and the energy efficient version of the building (there referred as the improved state). In general, the results agree with the outputs of section 5.1, where it was concluded that the MM5 datasets tend to underestimate the temperature parameter and to simulate shorter time variability for most of the climate parameters. In fact, the results of dynamic simulations recorded the lowest overheating rates and the highest heating needs. Nonetheless, all the models delivered similar results in the annual assessment.

In the thermal comfort evaluation (Figure 11 and Figure 12), the results for the CORDEX datasets, both HadRM3P and RCA4 delivered similar results. In regards to the CORDEX-HadRM3P dataset, the highest overheating rates were recorded which agrees with the previous results considering that in the analysis of the monthly mean temperatures, this dataset tends to overestimate the temperature parameter. Similar results were seen in the MM5 datasets where just minor differences were found comparing the results for MRF-NOAH and PLEIM-XIU. Regarding the results employing the DB dataset, even though it had the poorest outcomes in the intercomparison of hourly values (Taylor diagrams), just minor differences were detected in the annual thermal comfort assessment when compared with the results employing the other datasets. This is due to the fact that when analysing the results in terms of temperature differences (Figure 4b), the accuracy of the models in describing the temperature pattern changes according to the months since the models alternately underestimate or overestimate it. This involves changes in the distribution of overheating or underheating rates. In addition, when considering the annual results, the values tend to offset each other through the days resulting in a good estimation of the total comfort rates. To support this statement, the hottest and coldest week of the observed year were simulated, and the results are shown in Figure 14 regarding discomfort rates. All the datasets were able to describe a similar annual thermal performance of the building in the year under consideration and therefore represent a reliable tool to the building thermal comfort evaluation process on a yearly basis.

Even though this research did not intend to analyse the differences between the adaptive and the static approaches for thermal comfort evaluation, it is worth noting that when considering a fixed temperature range, independent of the outdoor conditions, the overheating rates are more significant for both the original state and the energy efficient version of the building. In fact, the underheating rates are less significant in the static approach, which was also confirmed by Barbosa et al.'s findings [91].

Furthermore, the adaptive approach tends to be permissive with high temperatures but not with low temperatures, since for example, for a running mean outdoor temperature of 26.4°C, the optimal operative temperature is 27.5°C, and the upper and lower limits are 30.5°C and 23.5°C respectively. In this way, an operative temperature of 22.0°C is recorded as an underheating rate, when in fact 22°C is between the comfort range of the static model. Finally, significant improvements in the

thermal performance of the building were reported when comparing the results in the original state with the energy efficiency version, where the use of thermal insulation in walls and roofs were quite effective in decreasing the discomfort rate of the building.
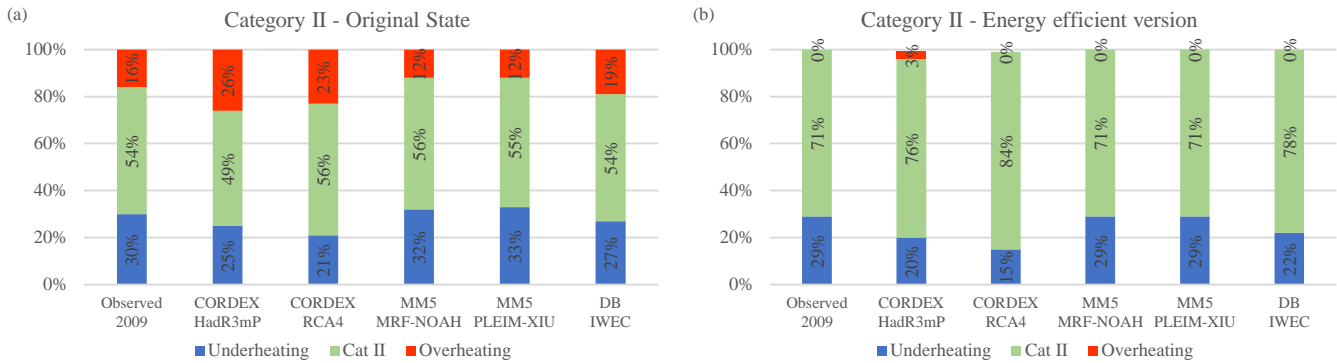

Figure 11 - Annual average comfort rates according to the adaptive thermal comfort approach of EN 15251, for the building in the original state (a) and in the energy efficient version (b).
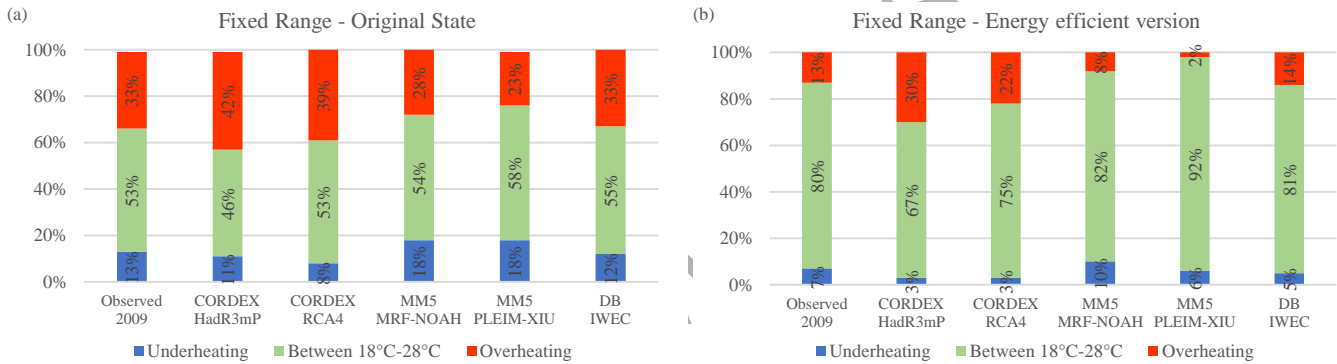

Figure 12 - Annual average comfort rates according to the static thermal comfort approach, for the building in the original state (a) and in the energy efficient version (b).

In Figure 13, the annual simulation underlines the ability of the climate models to estimate the total annual energy requirement for both the original and the improved state, especially in the case of MM5-MRF-NOAH, which delivered results with a very good approximation regarding the observed case. Nonetheless, both MM5 datasets tended to slightly overestimate the heating needs, which agrees with the thermal assessment analysis, considering that they delivered the highest underheating rates. The datasets overestimating the cooling needs correspond to those of CORDEX and DB, which also provided the highest overheating rates in the thermal assessment. Considering the improved state, the energy demand of the thermal zone decreased exponentially, showing the effectiveness of the energy efficient version of the building and confirming the recorded trend among all models. Thus, the annual energy requirement was also well estimated with the different weather datasets.

In this way, the differences between the weather datasets, which were detected in the statistic intercomparison of hourly values (section 5.1) were not reflected in the annual energy simulation results. As was previously referred, this is due to the fact that the models tend to overestimate or underestimate the temperature pattern throughout the year, affecting the distribution of

heating and cooling energy needs. Finally, on an annual basis, the results are offset resulting in a good estimation of the total annual energy requirement. To demonstrate this, Figure 15 depicts the energy requirement during the hottest and coldest week of the observed year, applying the different weather data files under analysis.
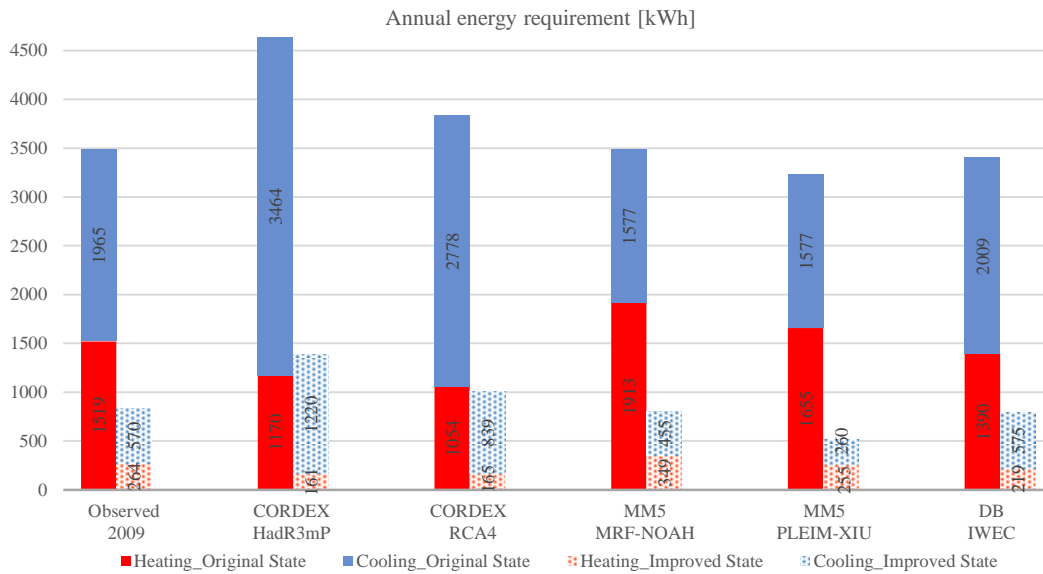

Figure 13 – Annual profiles of heating and cooling energy needs for the building in the original state and the energy efficient version.

According to the temperature records of the observed year, the hottest week corresponds to the period of 30th October to 5th November (spring season) and the coldest week corresponds to the period of 21st to 27th July (winter season). For the weekly comfort assessment, the results refer to the building in the original state, considering that the same trend was detected in the simulations of the building in the energy efficient version. Furthermore, the results are depicted employing the statistic approach, using fixed threshold values of comfort temperature, since the adaptive approach, as the name suggests, tends to adapt the comfort rates according to the outdoor temperatures, and the objective of this analysis is to underline the impact of the surrounding climate on the comfort rates. For both simulated weeks, the less accurate results corresponded to the dataset of DB.
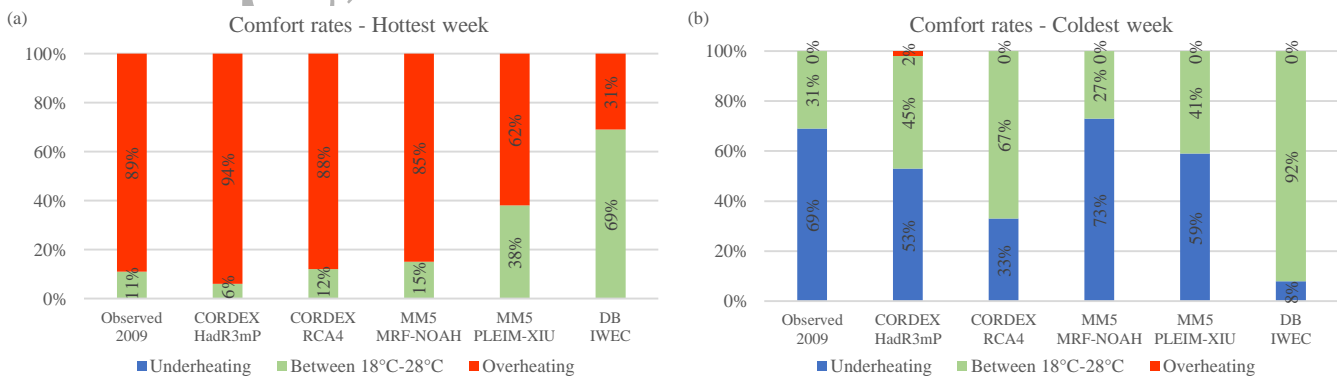

Figure 14 – Weekly profiles of discomfort rates for the building in the original state for (a) the hottest and (b) the coldest week of the observed year.

Figure 14a depicts the results for the hottest week, which was recorded in the spring season. According to the intercomparison regarding hourly values (Taylor diagrams – Figure 3a), DB was the poorest performing model in this season. This result was also confirmed in the thermal comfort evaluation, where the observed dataset delivered an overheating rate of 89% while DB recorded a rate of just 31%. The same performance was detected for the coldest week (Figure 14b), where the observed dataset recorded an underheating rate of 69% while DB (which considered the building in comfort almost all the time) recorded an underheating rate of just 8%.

In the hottest week, all the other models were able to estimate with a good approximation the overheating rates of the buildings, though the MM5-PLEIM-XIU dataset resulted a little less accurate. Although this dataset presented good performance in the intercomparison of hourly values, with slightly lower RMSD and higher correlations, it tended to simulate a shorter time variability of the temperature parameter, describing the pattern well but losing all the peaks, being this last one very influential in the comfort rates. According to the intercomparison of hourly values for the winter season (Taylor diagram – Figure 3c), the poorest performing model in this season corresponded to DB followed by CORDEX-RCA4, which is also underlined in Figure 14b.

Figure 15 depicts the energy needs of the thermal zone under analysis for the hottest and coldest week of the observed year, considering both the original state and the energy efficient version of the building (there referred as the improved state). Through the analysis of the energy requirement, the same trend in the comfort assessment was noticed, where the DB dataset greatly delivered the poorest results when compared with observations. Furthermore, although in the comfort assessment the different weather datasets delivered very similar comfort rates, in terms of energy requirements, the differences between them were better understood.
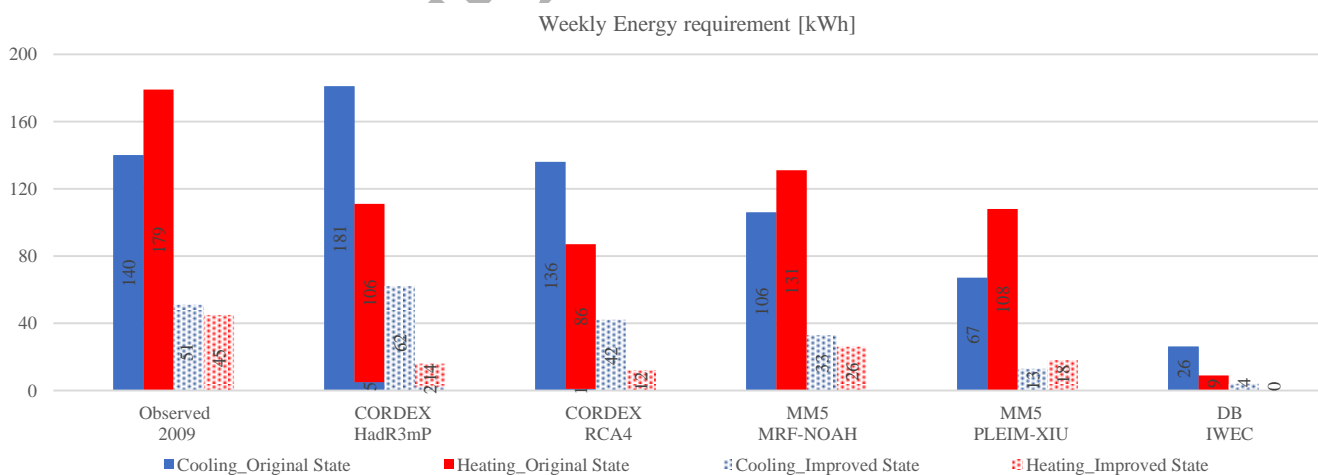

Figure 15- Weekly profiles of heating and cooling energy needs for the building in the original state and the energy efficient version.

In general, the CORDEX models tend to simulate better during the warmer periods and those of MM5 during the colder periods. Nonetheless, the model simulating the best approximation in both weeks was the MM5-MRF-NOAH model, which also had a good performance in the intercomparison of hourly values and the annual energy simulations, both for comfort and

energy requirement assessment. Thus, if these weeks are used for the calibration of buildings energy models, and real energy consumption data are compared, the DB datasets would have a significant impact on the results and the datasets obtained from the regional climate models could be a better option.

7. Conclusions

The aim of this research work was to investigate the possibility of using weather data files obtained from meteorological models for building energy simulations and, in particular, as a substitute of real data for calibration purposes. Comparisons in terms of comfort condition and energy demand in relation to the results obtained from real meteorological data of a specific year were carried out. Six weather datasets obtained from different sources were analysed, which correspond to four regional climate models (MM5 MRF-NOAH & MM5 PLEIM-XIU and CORDEX HadRM3P & CORDEX RCA4), the default IWEC weather data file available in DesignBuilder and the real data collected from measurements at the Silvio Pettirossi Airport.

The first stage of the analysis concerned an intercomparison between the main climate parameters (temperature, atmospheric pressure, relative humidity, wind speed and direction, cloud cover) which were measured and simulated for the city of Asunción. The second analysis concerned the estimation of direct and diffused components of global solar radiation evaluated by the numerical models, using existing empirical correlation models for the Brazilian city of São Martinho da Serra, which was chosen for the availability of recorded data of solar radiation.

Thus, the three main targets were: to determine the accuracy of the climate models to describe climatology of the cities under study; to evaluate the accuracy of the estimation of global solar radiation and the use of empirical correlation models, aiming to present alternatives to solve the problem of missing data; and finally, to quantify the influence of measured/simulated meteorological data on the evaluation of building thermal performance.

The main conclusions of the investigation are summarised as follows:

- For the intercomparison among weather datasets relating to the city of Asunción, in general the climate models tend to perform better the climate parameters of temperature and atmospheric pressure than the others. The CORDEX datasets perform better than those of MM5 in relation to time distribution, though deliver slightly lower RMSD and higher correlations, and tend to underestimate all the climate parameters generally. Overall, the models performing slightly better were CORDEX-HadRM3P and MM5-MRF-NOAH, which behaved similarly on an annual basis and statistically, for each parameter, they demonstrated slightly better skills in depicting time distribution, RMSD and correlation values. In general, the regional climate models' skills were good and they were able to describe the surface climatology of Asunción in the year under study, especially concerning the temperature pattern. When referring to a typical meteorological year compared to a specific year (2009), the DB dataset always presented the lowest correlations and highest RMSD values.

- For the intercomparison between weather datasets relating to São Martinho da Serra, the regional climate models described the global solar radiation pattern well, presenting very similar results. The Campbell & Norman methodology, though not

31

as accurate as the regional climate models, is an alternative for estimating this parameter on the basis of available measured data regarding temperature, relative humidity and atmospheric pressure. In regards to the correlation models used to decompose global solar radiation into its diffused and direct components, the direct solar radiation parameter was analysed, and in general, all the correlation models estimated a low time variability of the parameter, presenting very similar results. Nonetheless, the correlation model developed by Marques et al. [86] was able to describe the time variability of the parameter during the seasons slightly better and the whole year for the city under analysis, recording slightly higher correlation coefficients.

- For the building energy simulations regarding annual data, all the results using the different weather datasets were similar, also when compared to the results of the reference (observed dataset). This is due to the fact that the accuracy of the models in describing the temperature pattern changes according to the months since the models alternately underestimate or overestimate it. When considering the annual results, the values tend to offset each other through the days resulting in a good estimation of the total comfort rates and the total annual energy requirement. Nonetheless, as the calibration of building energy models is usually carried out for simulation periods lasting less than a year, weekly analyses were performed. Hence, the inaccuracy of the DB dataset was accentuated in the weekly analyses, where the results of the intercomparison of hourly values are confirmed. The regional climate models, especially the MM5-MRF-NOAH, showed high reliability in the estimation of the energy requirements and comfort rates. Thus, the results obtained in this paper suggest that the weather datasets obtained from regional climate models represent a reliable tool for building energy performance assessment, and mainly for the calibration of building energy models when measured weather data is not available.

Based on the above conclusions, the weather data files used for the dynamic energy simulations can affect the results of the building energy performance significantly, especially for simulation periods lasting less than a year. Nonetheless, simulated meteorological data has shown to be a reliable option when observed data is unavailable. In addition, the use of regional climate models to build a typical meteorological year, simulating a considerable period of years, could represent a reliable strategy to be implemented in the dynamic energy simulations of buildings.

It is important to highlight that the methodology presented here can be applied to any location on the globe since regional climate models cover every location, and the accuracy of the models is continuously improving. In fact, the authors are working on applying this methodology for research on cities located in the northern hemisphere. Regarding the main challenges, the availability of observed weather data to evaluate the accuracy of the models could be considered as the main limitation. The analysis of more than a single year could be recommended to give even more reliability to the results. Nonetheless, this research provides a scientifically based approach to analyse the important role played by weather datasets on building energy simulation outputs, the accuracy of different weather datasets obtained from regional climate models and finally, the accuracy of correlation models to decompose global solar radiation data into its direct and diffused components.

8. Acknowledgements

9. References

[1]   O. Lucon, D. Ürge-Vorsatz, A. Zain Ahmed, H. Akbari, P. Bertoldi, L.F. Cabeza, N. Eyre, A. Gadgil, L.D.D. Harvey, Y. Jiang, E. Liphoto, S. Mirasgedis, S. Murakami, J. Parikh, C. Pyke, M.V. Vilariño, Buildings, Clim. Chang. 2014 Mitig. Clim. Chang. Contrib. Work. Gr. III to Fifth Assess. Rep. IPCC. (2014) 671–738. doi:10.2753/JES1097-203X330403.

[2]   P. Chalmers, Climate Change: Implications for Buildings, Cambridge, United Kingdom, 2014.

[3]   M. Levine, D. Ürge-Vorsatz, K. Blok, L. Geng, D. Harvey, S. Lang, G. Levermore, A.M. Mehlwana, S. Mirasgedis, A. Novikova, J. Rilling, H. Yoshino, O.R. Davidson, P.R. Bosch, R. Dave, Residential and commercial buildings, Clim. Chang. 2007 Mitigation, Contrib. Work. Gr. III to Fourth Assess. Rep. IPCC. (2007) 387–446.

[4]   K. Lee, H. Yoo, G.J. Levermore, Generation of typical weather data using the ISO Test Reference Year (TRY) method for major cities of South Korea, Build. Environ. 45 (2010) 956–963. doi:10.1016/j.buildenv.2009.10.002.

[5]   A. Mahdavi, V. Leinich, K. Orehounig, Implications of varying weather data sets for predictions of thermal performance of buildings, PLEA 2008 – 25th Conf. Passiv. Low Energy Archit. (2008).

[6]   Y. Ding, Y. Shen, J. Wang, X. Shi, Uncertainty sources and calculation approaches for building energy simulation models, Energy Procedia. 78 (2015) 2566–2571. doi:10.1016/j.egypro.2015.11.283.

[7]   H. Radhi, A comparison of the accuracy of building energy analysis in Bahrain using data from different weather periods, Renew. Energy. 34 (2009) 869–875. doi:10.1016/j.renene.2008.06.008.

[8]   J. Taylor, M. Davies, A. Mavrogianni, Z. Chalabi, P. Biddulph, E. Oikonomou, P. Das, B. Jones, The relative importance of input weather data for indoor overheating risk assessment in dwellings, Build. Environ. 76 (2014) 81–91. doi:10.1016/j.buildenv.2014.03.010.

[9]   D. Ciobanu, E. Eftimie, C. Jaliu, The influence of measured/simulated weather data on evaluating the energy need in buildings, Energy Procedia. 48 (2014) 796–805. doi:10.1016/j.egypro.2014.02.092.

[10]   Energy Plus Software, Weather data sources, (n.d.). https://energyplus.net/weather/sources (accessed February 27, 2018).

[11]   J. Remund, S. Müller, S. Kunz, B. Huguenin-Landl, C. Studer, R. Cattin, Meteonorm Handbook, Version 7., METEOTEST, Bern, Switzerland, 2017.

[12]   S.A. Klein, D.W.A. Beckman, D.J.A. Duffie, TRNSYS - a transient simulation program, 16th ed., Solar Energy Laboratory, University of Wisconsin-Madison, Madison, WI 53706 – U.S.A., 2007.

[13]   M. Petrakis, P. Lykoudis, P. Kassomenos, A software tool for the creation of a typical meteorological year, Environ. Softw. 11 (1996) 221–227. doi:10.1016/j.renene.2008.05.046.

[14]   L. Adelard, H. Boyer, F. Garde, J.C. Gatina, Detailed weather data generator for building simulations, Energy Build. 31 (2000) 75–88. doi:10.1016/S0378-7788(99)00009-2.

[15]   D. Johansson, Comparison between synthetic outdoor climate data and readings – Applicability of Meteonorm in Sweden for building simulations, System. (2008) 17–22.

[16]   M. Bhandari, S. Shrestha, J. New, Evaluation of weather datasets for building energy simulation, Energy Build. 49 (2012) 109–118. doi:10.1016/j.enbuild.2012.01.033.

[17]   S. Erba, F. Causone, R. Armani, The effect of weather datasets on building energy simulation outputs, Energy Procedia. 134 (2017) 545–554. doi:10.1016/j.egypro.2017.09.561.

[18]   G. Chiesa, M. Grosso, The influence of different hourly typical meteorological years on dynamic simulation of buildings, Energy Procedia. 78 (2015) 2560–2565. doi:10.1016/j.egypro.2015.11.280.

[19]   G. Murphy, F. Monari, Determining the effect of weather data upon building simulation in regulatory processes, in: 13th Conf. Int. Build. Perform. Simul. Assoc., Chambéry, France, 2013: pp. 946–953.

[20]   T.A. Reddy, Literature Review on Calibration of Building Energy Simulation Programs, ASHRAE Trans. 112 (2006) 226–240.

[21]   A. Chong, K. Menberg, Guidelines for the Bayesian calibration of building energy models, Energy Build. 174 (2018) 527–547. doi:https://doi.org/10.1016/j.enbuild.2018.06.028.

[22]   Y. Heo, D.J. Graziano, L. Guzowski, R.T. Muehleisen, Evaluation of calibration efficacy under different levels of uncertainty, J. Build. Perform. Simul. 8 (2015) 135–144. doi:10.1080/19401493.2014.896947.

[23]   K. Menberg, Y. Heo, R. Choudhary, Influence of error terms in Bayesian calibration of energy system models, J. Build. Perform. Simul. 1493 (2018) 1–15. doi:10.1080/19401493.2018.1475506.

[24]   B. Eisenhower, Z. O'Neill, V.A. Fonoberov, I. Mezić, Uncertainty and sensitivity decomposition of building energy models, J. Build. Perform. Simul. 5 (2012) 171–184. doi:10.1080/19401493.2010.549964.

[25]   Y. Sun, Y. Heo, M. Tan, H. Xie, C.F. Jeff Wu, G. Augenbroe, Uncertainty quantification of microclimate variables in building energy models, J. Build. Perform. Simul. 7 (2014) 17–32. doi:10.1080/19401493.2012.757368.

[26]   National Institute for Space Research, SONDA, Brazilian Environmental Data Organization System, (n.d.). http://sonda.ccst.inpe.br/ (accessed March 16, 2018).

[27]   K.E. Taylor, Taylor Diagram Primer, Work. Pap. (2005) 1–4. doi:10.1029/2000JD900719.

[28]   G. Tang, Z. Zeng, D. Long, X. Guo, B. Yong, W. Zhang, Y. Hong, Statistical and Hydrological Comparisons between TRMM and GPM Level-3 Products over a Midlatitude Basin: Is Day-1 IMERG a Good Successor for TMPA 3B42V7?, J. Hydrometeorol. 17 (2016) 121–137. doi:10.1175/JHM-D-15-0059.1.

[29]   X. Niu, S. Wang, J. Tang, D. Lee, W. Gutowski, K. Dairaku, J. Mcgregor, J. Katzfey, X. Gao, J. Wu, S. Hong, Y. Wang, H. Sasaki, Journal of Geophysical Research : Atmospheres, 3 (2015) 1–18. doi:10.1002/2014JD022620.Received.

[30]   M. Despotovic, V. Nedic, D. Despotovic, S. Cvetanovic, Evaluation of empirical models for predicting monthly mean horizontal diffuse solar radiation, Renew. Sustain. Energy Rev. 56 (2016) 246–260. doi:10.1016/j.rser.2015.11.058.

[31]   T. Kärnä, A.M. Baptista, Evaluation of a long-term hindcast simulation for the Columbia River estuary, Ocean Model. 99 (2016) 1–14. doi:10.1016/j.ocemod.2015.12.007.

[32]   R. Barlow, Statistics - A guide to the use of statistical methods in the physical sciences, John Wiley & Sons, Baffins Lane, Chichester, 2013.

[33]   F. Gravetter, L. Wallnau, Essentials of Statistics for the Behavioral Science, 6th ed., Thomson Wadsworth, 2008.

[34]   K.E. Taylor, Summarizing multiple aspects of model performancein a single diagram, J. Geophys. Res. 106 (2001) 7183–7192.

[35]   M. Lange, U. Focken, Physical Approach to Short-TermWind Power Prediction, Springer, Berlin, 2006.

[36]   Big Ladder Software, Elements, Rocky Mt. Inst. (2017).

[37]   European Committee for Standardization (CEN), EN 15251: Indoor environmental input parameters for the design and assessment of energy performance of buildings, (2014) 1–81. doi:CEN/TC 156WG19-N77. STD Version 2.1c.

[38]   S. Carlucci, L. Bai, R. de Dear, L. Yang, Review of adaptive thermal comfort models in built environmental regulatory documents, Build. Environ. 137 (2018) 73–89. doi:10.1016/j.buildenv.2018.03.053.

[39]   C.A. Alves, D.H.S. Duarte, F.L.T. Gonçalves, Residential buildings' thermal performance and comfort for the elderly under climate changes context in the city of São Paulo, Brazil, Energy Build. 114 (2016) 62–71. doi:10.1016/j.enbuild.2015.06.044.

[40]   A. Figueiredo, J. Figueira, R. Vicente, R. Maio, Thermal comfort and energy performance: Sensitivity analysis to apply the Passive House concept to the Portuguese climate, Build. Environ. 103 (2016) 276–288. doi:10.1016/j.buildenv.2016.03.031.

[41]   A. Roetzel, A. Tsangrassoulis, Impact of climate change on comfort and energy performance in offices, Build. Environ. 57 (2012) 349–361. doi:10.1016/j.buildenv.2012.06.002.

[42]   A. Figueiredo, R. Vicente, J. Lapa, C. Cardoso, F. Rodrigues, J. Kämpf, Indoor thermal comfort assessment using different constructive solutions incorporating PCM, Appl. Energy. 208 (2017) 1208–1221. doi:10.1016/j.apenergy.2017.09.032.

[43]   A. Roetzel, A. Tsangrassoulis, U. Dietrich, Impact of building design and occupancy on office comfort and energy performance in different climates, Build. Environ. 71 (2014) 165–175. doi:10.1016/j.buildenv.2013.10.001.

[44]   C. Rubio-Bellido, A. Pérez-Fargallo, J.A. Pulido-Arcas, M. Trebilcock, Application of adaptive comfort behaviors in Chilean social housing standards under the influence of climate change, Build. Simul. 10 (2017) 933–947. doi:10.1007/s12273-017-0385-9.

[45]   Ministerio da Economia e do Emprego, Decreto Lei N° 118/2013 de 20 de Agosto - Regulamento de Desempenho Energetico dos Edifícios de Habitaçao (REH), (2013) 4988–5005.

[46]   Ministerio de Vivienda y Urbanismo del Gobierno de Chile, Estándares de Construcción Sustentable para viviendas de Chile, Tomo I: Salud y Bienestar, Second, Santiago de Chile, 2018.

[47]   Brazilian Association of Technical Standards (ABNT), NBR 16401:2008 Instalações de ar-condicionado - Sistemas centrais e unitários - Parte 2: Parâmetros de conforto térmico., (2008).

[48]   Chartered Institution of Building Services Engineers (CIBSE), Environmental design, 7th ed., London, 2006. doi:10.1016/B978-0-240-81224-3.00016-9.

[49]   S. Lu, B. Pang, Y. Qi, K. Fang, Field study of thermal comfort in non-air-conditioned buildings in a tropical island climate, Appl. Ergon. 66 (2018) 89–97. doi:10.1016/j.apergo.2017.08.008.

[50]   H. Djamila, Indoor thermal comfort predictions: Selected issues and trends, Renew. Sustain. Energy Rev. 74 (2017) 569–580. doi:10.1016/j.rser.2017.02.076.

[51]   V. López, J.R. Lucchese, W.A. Andreasi, Thermal Comfort Assessment in the Hot and Humid Region of Paraguay : a Comparison Between Three Methodologies, (2015) 26–31.

[52]   Secretary of the Environment of Paraguay (SEAM), Primera Comunicación Nacional a la Convención Marco de las Naciones Unidas sobre Cambio Climático, First, AGR Servicios Graficos, Asuncion, Paraguay., 2001.

[53]   M.C. Peel, B.L. Finlayson, T.A. McMahon, Updated world map of the Köppen-Geiger climate classification, Hydrol. Earth Syst. Sci. Discuss. 4 (2007) 439–473. doi:10.5194/hessd-4-439-2007.

[54]   G. Grell, J. Dudhia, D. Stauffer, A description of the Fifth-generation Penn State/NCAR Mesoscale Model (MM5), 1994. doi:10.5065/D60Z716B.

[55]   J. Dudhia, D. Gill, K. Manning, W. Wang, C. Bruyere, S. Kelly, K. Lackey, PSU / NCAR Mesoscale Modeling System Tutorial Class Notes and User ' s Guide : MM5 Modeling System Version 3, Mesoscale and Microscale Meteorology Division National Center for Atmospheric Research, 2005.

[56]   S.-Y. Hong, H.-L. Pan, Nonlocal Boundary Layer Vertical Diffusion in a Medium-Range Forecast Model, Mon. Weather Rev. 124 (1996) 2322–2339. doi:10.1175/1520-0493(1996)124<2322:NBLVDI>2.0.CO;2.

[57]   J.E. Pleim, J.S. Chang, A non-local closure model for vertical mixing in the convective boundary layer, Atmos. Environ. Part A, Gen. Top. 26 (1992) 965–981. doi:10.1016/0960-1686(92)90028-J.

[58]   A. Xiu, J.J.E.J. Pleim, Development of a land surface model. Part I: Application in a mesoscale meteorological model, J. Appl. Meteorol. 40 (2001) 192–209. doi:10.1175/1520-0450(2001)040<0192:DOALSM>2.0.CO;2.

[59]   F. Giorgi, C. Jones, G.R. Asrar, Addressing climate information needs at the regional level: The CORDEX framework, World Meteorol. Organ. Bull. 58 (2009) 175–183.

[60]   P. Samuelsson, Using regional climate models to quantify the impact of climate change on lakes, in: G. Glen (Ed.), Impact Clim., Springer, London New York, 2010: pp. 15–32.

[61]   S. Kotlarski, K. Keuler, O.B. Christensen, A. Colette, M. Déqué, A. Gobiet, K. Goergen, D. Jacob, D. Lüthi, E. Van Meijgaard, G. Nikulin, C. Schär, C. Teichmann, R. Vautard, K. Warrach-Sagi, V. Wulfmeyer, Regional climate modeling on European scales: A joint standard evaluation of the EURO-CORDEX RCM ensemble, Geosci. Model Dev. 7 (2014) 1297–1333. doi:10.5194/gmd-7-

1297-2014.

[62]   P. Berrisford, D. Dee, K. Fielding, M. Fuentes, P. Kallberg, S. Kobayashi, S. Uppala, The ERA-Interim Archive, ERA Rep. Ser. 1 (2009) 1–16. http://www.ecmwf.int/publications/library/do/references/list/782009.

[63]   DesignBuilder Software Ltd, DesignBuilder EnergyPlus Simulation Documentation for DesignBuilder v5, 2015. www.designbuilder.co.uk.

[64]   American Society of Heating Refrigeration and Air Conditioning Engineers (ASHRAE), International Weather for Energy Calculations (IWEC Weather Files) Users Manual and CD-ROM, Atlanta, EEUU., 2001.

[65]   A. Ben Jemaa, S. Rafa, N. Essounbouli, A. Hamzaoui, F. Hnaien, F. Yalaoui, Estimation of global solar radiation using three simple methods, Energy Procedia. 42 (2013) 406–415. doi:10.1016/j.egypro.2013.11.041.

[66]   M.H. Soulouknga, O. Coulibaly, S.Y. Doka, T.C. Kofane, Evaluation of global solar radiation from meteorological data in the Sahelian zone of Chad, Renewables Wind. Water, Sol. 4 (2017) 4. doi:10.1186/s40807-017-0041-0.

[67]   A.K. Doost, M. Akhlaghi, Estimation and Comparison of Solar Radiation Intensity by Some Models in a Region of Iran, J. Power Energy Eng. 2 (2010) 345–351. doi:10.4236/jpee.2014.24046.

[68]   A. De Rosa, V. Ferraro, D. Kaliakatsos, V. Marinelli, Simplified correlations of global, direct and diffuse luminous efficacy on horizontal and vertical surfaces, Energy Build. 40 (2008) 1991–2001. doi:10.1016/j.enbuild.2008.04.018.

[69]   S. Janjai, M. Nunez, J. Prathumsit, R. Wattan, R. Sabooding, A semi-empirical approach for the estimation of global, direct and diffuse illuminance under clear sky condition in the tropics, Energy Build. 66 (2013) 177–182. doi:10.1016/j.enbuild.2013.07.003.

[70]   S. Kaynak, B. Kaynak, A. Özmen, A software tool development study for solar energy potential analysis, Energy Build. 162 (2018) 134–143. doi:10.1016/j.enbuild.2017.12.033.

[71]   L. Robledo, A. Soler, Estimation of global illuminance for clear skies at Madrid, Energy Build. 31 (2000) 25–28. doi:10.1016/S0378-7788(98)00071-1.

[72]   D. Vázquez, E. Bernabeu, Quantitative estimation of clear sky light in Madrid, Energy Build. 26 (1997) 331–336.

[73]   G. Lupato, M. Manzan, S. Cirilli, Comparison of Direct Radiation Split Algorithms for Energy Simulation of Buildings, in: Build. Simul. Appl. BSA 2017, 2017: pp. 233–240. doi:10.1534/g3.116.033225.

[74]   A. Teke, H.B. Yildirim, Ö. Çelik, Evaluation and performance comparison of different models for the estimation of solar radiation, Renew. Sustain. Energy Rev. 50 (2015) 1097–1107. doi:10.1016/j.rser.2015.05.049.

[75]   F. Besharat, A.A. Dehghan, A.R. Faghih, Empirical models for estimating global solar radiation: A review and case study, Renew. Sustain. Energy Rev. 21 (2013) 798–821. doi:10.1016/j.rser.2012.12.043.

[76]   G. Campbell, J. Norman, An Introduction to Environmental Biophysics, Second, Springer- Verlag, New York, United States, 1998. doi:10.2134/jeq1977.00472425000600040036x.

[77]   The Chartered Institution of Building Services Engineers, Solar radiation , longwave radiation and daylight, CIBSE Guid. A. (2015).

[78]   D.F. Al Riza, S.I. Haq Gilani, M. Shiraz Aris, Hourly solar radiation estimation using ambient temperature and relative humidity data, Int. J. Environ. Sci. Dev. 2 (2011) 188–193. doi:10.7763/IJESD.2011.V2.122.

[79]   K. Spokas, F. Forcella, Estimating hourly incoming solar radiation from limited meteorological data, Weed Sci. 54 (2006) 182–189. doi:10.1614/WS-05-098R.1.

[80]   B. Liu, C. Jordan, The interrelationship and Characteristic Distribuition of Direct, diffuse and Total solar radiation, (1960) 19.

[81]   J.A. Duffie, W.A. Beckman, Solar Engineering of Thermal Processes Solar Engineering, 2013. doi:10.1002/9781118671603.fmatter.

[82]   R. Tapakis, S. Michaelides, A.G. Charalambides, Computations of diffuse fraction of global irradiance: Part 2 – Neural Networks, Sol. Energy. 139 (2016) 723–732. doi:10.1016/j.solener.2015.12.042.

[83]   D. Erbs, S. Klein, J. Duffie, Estimation of the diffuse radiation fraction for hourly, daily and monthly-average global radiation, Sol. Energy. 28 (1982) 293–302. doi:https://doi.org/10.1016/0038-092X(82)90302-4.

[84]   J. Orgill, K. Hollands, Correlation equation for hourly diffuse radiation on a horizontal surface, Sol. Energy. 19 (1977) 357–359. doi:https://doi.org/10.1016/0038-092X(77)90006-8.

[85]   M. Chikh, A. Mahrane, M. Haddadi, Modeling the diffuse part of the global solar radiation in Algeria, Energy Procedia. 18 (2012) 1068–1075. doi:10.1016/j.egypro.2012.05.121.

[86]   E.P. Marques Filho, A.P. Oliveira, W.A. Vita, F.L.L. Mesquita, G. Codato, J.F. Escobedo, M. Cassol, J.R.A. França, Global, diffuse and direct solar radiation at the surface in the city of Rio de Janeiro: Observational characterization and empirical modeling, Renew. Energy. 91 (2016) 64–74. doi:10.1016/j.renene.2016.01.040.

[87]   B. Ridley, J. Boland, P. Lauret, Modelling of diffuse solar fraction with multiple predictors, Renew. Energy. 35 (2010) 478–483. doi:10.1016/j.renene.2009.07.018.

[88]   L.F.L. Lemos, A.R. Starke, J. Boland, J.M. Cardemil, R.D. Machado, S. Colle, Assessment of solar radiation components in Brazil using the BRL model, Renew. Energy. 108 (2017) 569–580. doi:10.1016/j.renene.2017.02.077.

[89]   Facultad de Arquitectura de la Universidad Nacional de Asunción, Análisis de la situacion actual del Centro Histórico de la ciudad de Asunción, Banco Interamericano de Desarrollo, Asunción, Paraguay., 2005.

[90]   P. Wankanapon, R.G. Mistrick, Roller Shades and Automatic Lighting Control with Solar Radiation Control Strategies, Built. 1 (2011) 35–42. doi:10.14456.

[91]   R. Barbosa, R. Vicente, R. Santos, Climate change and thermal comfort in Southern Europe housing: A case study from Lisbon, Build. Environ. 92 (2015) 440–451. doi:10.1016/j.buildenv.2015.05.019.